

## Fixed Anvil Temperature Feedback: Positive, Zero, or Negative?

MASAKAZU YOSHIMORI

*Faculty of Environmental Earth Science, Global Institution for Collaborative Research and Education, and Arctic Research Center, Hokkaido University, Sapporo, and Atmosphere and Ocean Research Institute, The University of Tokyo, Kashiwa, Japan*

F. HUGO LAMBERT

*College of Engineering, Mathematics and Physical Sciences, University of Exeter, Exeter, United Kingdom*

MARK J. WEBB AND TIMOTHY ANDREWS

*Met Office Hadley Centre, Exeter, United Kingdom*

(Manuscript received 8 February 2019, in final form 13 November 2019)

### ABSTRACT


The fixed anvil temperature (FAT) theory describes a mechanism for how tropical anvil clouds respond to global warming and has been used to argue for a robust positive longwave cloud feedback. A constant cloud anvil temperature, due to increased anvil altitude, has been argued to lead to a “zero cloud emission change” feedback, which can be considered positive relative to the negative feedback associated with cloud anvil warming when cloud altitude is unchanged. Here, partial radiative perturbation (PRP) analysis is used to quantify the radiative feedback caused by clouds that follow the FAT theory (FAT–cloud feedback) and to set this in the context of other feedback components in two atmospheric general circulation models. The FAT–cloud feedback is positive in the PRP framework due to increasing anvil altitude, but because the cloud emission does not change, this positive feedback is cancelled by an equal and opposite component of the temperature feedback due to increasing emission from the cloud. To incorporate this cancellation, the thermal radiative damping with fixed relative humidity and anvil temperature (T-FRAT) decomposition framework is proposed for longwave feedbacks, in which temperature, fixed relative humidity, and FAT–cloud feedbacks are combined. In T-FRAT, the cloud feedback under the FAT constraint is zero, while that under the proportionately higher anvil temperature (PHAT) constraint is negative. The change in the observable cloud radiative effect with FAT–cloud response is also evaluated and shown to be negative due to so-called cloud masking effects. It is shown that “cloud masking” is a misleading term in this context, and these effects are interpreted more generally as “cloud climatology effects.”

## 1. Introduction

The fixed-anvil temperature (FAT) theory, first proposed by [Hartmann and Larson \(2002\)](#), argues that tropical deep convective cloud anvil temperatures remain approximately constant as the climate warms, making tropical outgoing longwave radiation (OLR) for the cloudy sky depend little on the increasing surface

temperature. In the tropical average, the detrainment altitude of deep convective clouds corresponds to the divergence of vertical mass flux in the subsidence region, assuming that the outflow from the large-scale upwelling circulation, in which convection is embedded, occurs near the cloud detrainment level. In radiative convective equilibrium (RCE), the adiabatic warming accompanied by downward motion is balanced by radiative cooling, and thus the altitude of vertical divergence approximately coincides with a sharp vertical gradient of the radiative cooling profile. Under the fixed relative humidity (RH) assumption, the level of this sharp vertical gradient is determined by the saturation vapor pressure or equivalently by temperature. As a result, the

---

 Denotes content that is immediately available upon publication as open access.

---

*Corresponding author:* Masakazu Yoshimori, masakazu@aori.u-tokyo.ac.jp

DOI: 10.1175/JCLI-D-19-0108.1

© 2020 American Meteorological Society. For information regarding reuse of this content and general copyright information, consult the [AMS Copyright Policy \(www.ametsoc.org/PUBSReuseLicenses\)](#).

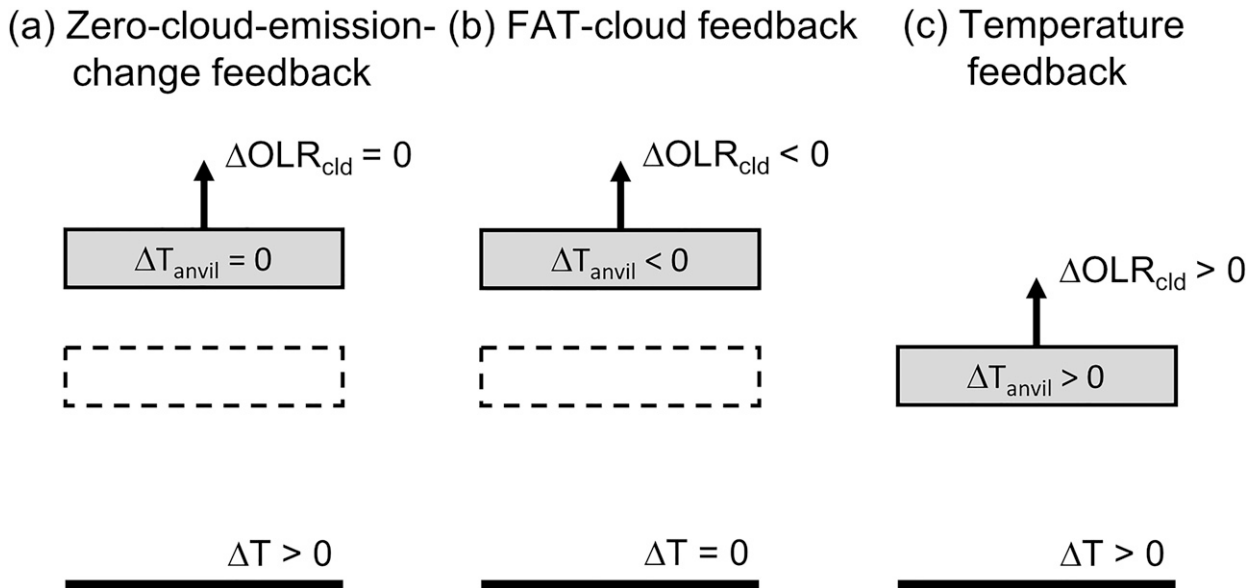


FIG. 1. Schematic illustration of different ways of diagnosing/interpreting the FAT effects on longwave climate feedbacks: (a) zero-cloud-emission-change feedback where two different states of temperature and cloud altitude between control and perturbed experiments are compared; (b) FAT-cloud feedback where radiative impact of only cloud altitude change is considered; (c) conventional temperature feedback where clouds stay at the same altitude.  $\Delta T$  and  $\Delta T_{\text{anvil}}$  denote changes in surface and troposphere temperature and cloud anvil temperature, respectively, and  $\Delta \text{OLR}_{\text{cld}}$  denotes outgoing longwave radiation change for the cloudy sky. Solid boxes represent anvil clouds and the dashed boxes represent their original altitude before elevated by the FAT mechanism.

outflow, detrainment, and anvil, which occur around a fixed temperature, shift to a higher altitude.

As noted in Boucher et al. (2013), it has long been recognized that climate feedback becomes more positive when clouds are raised in altitude compared to the case that clouds stay at the same altitude (Cess 1975; Cess et al. 1990; Hansen et al. 1984). Hartmann and Larson (2002) argue that if only the longwave (LW) emission were considered, tropical climate could be very sensitive to increasing surface temperatures, since LW emission from anvil clouds would not change greatly. However, they did not attempt to quantify the sign or magnitude of the FAT effect on climate feedbacks.

There are various arguments for the effect of the FAT mechanism on climate feedback described in the literature. Hartmann and Larson (2002) argue that cloud emission will not change greatly as the climate warms, which could be intuitively thought as a “zero cloud emission change” feedback (Fig. 1a). However, many studies argue that the FAT mechanism results in a positive feedback. Zelinka and Hartmann (2010) argue that the FAT mechanism provides a powerful constraint on the sign and magnitude of the LW cloud feedback in future climate change projections from general circulation models (GCMs). They demonstrated that the FAT-cloud response causes a positive feedback of clouds relative to the case when clouds stay at the same pressure level [fixed

anvil pressure (FAP)]. Soden and Vecchi (2011) argue that “The tendency of the tropical cirrus anvils to conserve cloud top temperature reduces the rate at which the TOA LW emission will increase in response to a surface warming and results in a positive feedback.” Bretherton (2015) argues that “FAT is a strong positive cloud feedback, because the infrared emission temperature of the cloud, and hence the overall LW radiative energy loss, is reduced by the upward shift of the cloud compared with the no-feedback case of a cloud which stays at the same altitude.” Boucher et al. (2013) state that “A positive feedback results because, since the cloud-top temperature does not keep pace with that of the troposphere, its emission to space does not increase at the rate expected for the no-feedback system,” while the exact definition of this “no-feedback system” is somewhat unclear. In the current study, we argue that the sign of LW feedback component associated with the FAT mechanism depends critically on the radiative feedback decomposition framework.

The LW component of the (total) climate feedback parameter can be approximately decomposed into a sum of individual feedback components:

$$\Lambda_{\text{LW}} = \Lambda_q + \Lambda_T + \Lambda_C, \quad (1)$$

where the subscripts  $q$ ,  $T$ , and  $C$  denote specific humidity, temperature, and cloud variables, respectively, and

$$\Lambda_x = \frac{\partial R}{\partial x} \frac{dx}{dT_s} \quad (x = q, T, C), \quad (2)$$

with  $R$  being LW radiative flux at the TOA (positive downward) and  $T_s$  the surface temperature (e.g., [Bony et al. 2006](#)). The temperature feedback may be further decomposed into the effect of vertically uniform temperature change (Planck) and the deviation from that uniform change (lapse rate). Positive feedback refers to the effect leading to an increase in net downward radiative flux at the TOA with warming ( $\Lambda_x > 0$ ). Here the feedback is defined in terms of changes in these specific quantities between two simulations, often constituting a tabulated summary of climate feedbacks (e.g., Table 9.5 and Fig. 9.43 in [Flato et al. 2013](#)). This approach allows the sign and magnitude of the LW cloud feedback, or a component of it, to be quantified. However, it should be noted that different interpretations will arise depending on which cloud variables are considered in  $C$ ; for example, the case where one considers changes in cloud temperature as part of the cloud feedback via  $C$  will give a very different decomposition to a case where changes in cloud temperature are treated as part of the temperature ( $T$ ) feedback ([Lambert et al. 2015](#)).

The cloud feedback has been quantified by the partial radiative perturbation (PRP) (e.g., [Colman and McAvaney 1997](#); [Wetherald and Manabe 1988](#); [Yoshimori et al. 2009](#)), its approximate descendant methods (e.g., [Shell et al. 2008](#); [Soden et al. 2008](#); [Taylor et al. 2007](#); [Yoshimori et al. 2011](#)), and, more recently, cloud radiative kernels with the ISCCP simulator output (e.g., [Chen et al. 2016](#); [Zelinka et al. 2012a,b, 2016](#)). [Zelinka and Hartmann \(2010\)](#) diagnosed the FAT component of cloud feedback for GCMs by first computing the cloud-related total feedback under the fixed high cloud temperature assumption in a simple model, and by later removing the cloud-related effect of temperature and water vapor feedbacks. All these methods are consistent with the definition of cloud feedback parameter in Eq. (2). In PRP, the radiative effect of clouds is evaluated through a radiative transfer calculation in which the cloud variables (e.g., cloud fraction, cloud water amount, and cloud particle size) from the reference and perturbed climates are exchanged while other noncloud variables are held fixed. Other noncloud feedbacks are evaluated consistently in much the same way. In the PRP diagnosis, the cloud temperature is assumed to be the same as that of the environment. That is, the change in the cloud temperature profile is not included in the variables perturbed when diagnosing the cloud feedback. Since the entire perturbed-climate cloud profile, including both the lifting of cloud in agreement with FAT and non-FAT changes in cloud properties, is used, it is difficult to isolate the FAT–cloud component. By lifting the cloud profile in accordance with

the expected FAT–cloud response to warming, in this study we are able to extract the FAT component of cloud feedback using an extension of the PRP method.

In general, the purpose of feedback analysis is to understand dominant processes in observed or simulated climate changes as well as to identify factors for model differences in response to perturbations. There is a convention in the way feedbacks are decomposed into individual components, although it is in principle arbitrary as long as it aids physical understanding. In the conventional PRP decomposition using specific humidity as a state variable, a partial cancellation occurs between the water vapor and the lapse rate feedbacks ([Colman 2003](#); [Soden and Held 2006](#)). As neither feedback correlates with the total feedback that determines the net response ([Ingram 2013](#)), it has been suggested that these two feedbacks should be treated collectively as a single feedback ([Randall et al. 2007](#)). While it is now understood that the partial cancellation occurs predominantly in the extratropics and arises from the two feedbacks being controlled commonly by the ratio of tropical to extratropical surface warming ([Po-Chedley et al. 2018](#)), the anticorrelation across models remains robust and the bundling of these feedbacks together is justified. [Ingram \(2010\)](#) proposed the “partly Simpsonian” component as a basic response in which it is assumed that effect of lapse rate, relative humidity, and pressure broadening on the clear-sky OLR do not change with temperature. Feedbacks to be analyzed are then defined with respect to the partly Simpsonian response. The basic response component is essentially built on the background (or mean) climate alone, and resulting feedbacks then do not show partial cancellation (having the same sign). The application of this new component widely to GCM diagnosis is, however, rather complicated, and [Ingram \(2012\)](#), [Held and Shell \(2012\)](#), and, more recently, [Caldwell et al. \(2016\)](#) suggested alternatively to use relative humidity as a state variable. There, the effect of water vapor change under the assumption of fixed RH is absorbed into the temperature component of feedbacks. We note that the partly Simpsonian response was recently updated by [Koll and Cronin \(2018\)](#) in which OLR emission through atmospheric Planck, lapse rate, and saturated water vapor feedbacks does not change with warming. In this article, we develop the idea of [Held and Shell \(2012\)](#) further and propose a new decomposition that includes both the fixed RH and FAT-induced radiative effects in the temperature feedback parameter. The new decomposition enables us to quantify the degree to which the intermodel differences are due to the difference in deviations from basic physical expectations of constant RH and FAT.

The radiative effect of clouds can also be quantified by the LW cloud radiative effect (CRE) defined as the difference between clear-sky and all-sky OLR. In models, the clear-sky flux is computed assuming no cloud in the radiative transfer calculations. While accurate understanding of the FAT component of cloud feedback comes from the PRP framework, we also evaluate the change in CRE ( $\Delta$ CRE) due to FAT–cloud response because CRE is a quasi-observable quantity, unlike PRP. In the present climate, the positive radiative effect of clouds in the LW arises from the lower cloud emission temperature compared to the higher effective emission temperature of the clear-sky region (Allan 2011). As  $\Delta$ CRE under the warming climate can be brought about by a change in the clear-sky flux,  $\Delta$ CRE may change even if the cloud variables (e.g., amount and optical properties) do not. Such an effect of noncloud variables on  $\Delta$ CRE has been termed “cloud masking” and is usually distinguished from the PRP cloud feedback, which represents the partial radiative effect due to the change in cloud variables alone (Soden et al. 2004; Zhang et al. 1994).  $\Delta$ CRE is mathematically equivalent to the sum of the PRP cloud feedback and the cloud masking effect on the noncloud PRP feedbacks (Soden et al. 2008). The physical interpretation of cloud masking is that clouds weaken the magnitude of noncloud feedbacks compared to what they would be in clear-sky conditions. In the process of evaluating the cloud masking component in  $\Delta$ CRE, we show that the term “cloud masking effect” can be misleading because the presence of cloud can enhance the magnitude of noncloud feedbacks and we argue that the term “impact of climatological clouds on noncloud feedbacks” (or “cloud climatology effect” for short) is more appropriate.

The FAT theory in its original and slightly modified forms [proportionately higher anvil temperature (PHAT), discussed in section 5] has been tested and verified against satellite cloud observations with sea surface temperature variations dominated by El Niño–Southern Oscillation (Eitzen et al. 2009; Xu et al. 2005, 2007; Zelinka and Hartmann 2011) and numerical experiments using cloud-resolving models in RCE (Harrop and Hartmann 2012; Kuang and Hartmann 2007). Some studies have questioned the accuracy of FAT (or PHAT) theory (Chae and Sherwood 2010; Li et al. 2012). In particular, Seeley et al. (2019a) pointed out weaknesses in FAT theory and argue that anvil temperatures can increase in a warmer climate. Seeley et al. (2019b) argue that the climatological anvil cloud amount is determined by the cloud evaporation rate, which may not be appropriately represented by GCMs. It is not the purpose of the current study to investigate the validity of FAT or PHAT theories. Rather, our aim is to quantify the contribution of the effect of elevating clouds, in agreement with FAT theory, to the overall climate

feedback in response to the tropospheric warming in two GCMs, taking into account all terms in a formal radiative feedback decomposition process.

Throughout the paper, we only discuss the LW component of the feedbacks. In the following, we refer to the hypothetically constructed cloud based on the FAT mechanism as FAT-induced cloud. We refer to the FAT component of cloud feedback, that is, altitude component of cloud feedback due to the difference between the FAT-induced cloud and the reference cloud, as FAT–cloud feedback (Fig. 1b). When this feedback is evaluated by PRP, it is referred to as FAT–cloud PRP. In the next section, models and experiments are briefly described. Section 3 explains how cloud variable changes following the FAT mechanism are constructed for PRP analysis and how the PRP analysis is performed. A brief description of radiative kernels, which are used to help interpret the PRP result, is also provided. The results are presented in section 4. Section 4a aims to quantify the FAT–cloud PRP. A new decomposition of feedbacks is proposed in section 4b, which aims to combine the cancelling feedback terms to enhance understanding of feedbacks. The impact of lapse rate changes on other feedbacks is also discussed. Section 4c aims to revisit the interpretation of the cloud masking effect in order to understand  $\Delta$ CRE with FAT–cloud response. Discussion and conclusions follow in sections 5 and 6, respectively.

## 2. Models and experiments

In the current study, two atmospheric general circulation models, MIROC5.2-A and HadGEM2-A, are used for a pair of AMIP and AMIP+4K experiments. These two experiments follow the CMIP5/CMIP6 protocol (Eyring et al. 2016; Taylor et al. 2012). In the AMIP experiment, historical forcings are applied and sea surface temperature and sea ice distribution based on observational data are used as time-varying lower boundary conditions. MIROC5.2-A with CMIP6 forcing and HadGEM2-A with CMIP5 forcing are integrated for 1979–2008. The AMIP experiment, therefore, is aimed to simulate atmospheric conditions as realistically as possible. In the AMIP+4K experiment, the SST is raised uniformly by 4°C, with other boundary conditions, including the historical forcing, identical to AMIP. Therefore, the difference between the two experiments provides only the surface temperature mediated response. All results presented in this article are annual averages over the entire model integration periods, unless noted otherwise.

MIROC5.2-A is a slightly updated version of MIROC5-A, an atmospheric component of the MIROC5 coupled

atmosphere–ocean general circulation model (AOGCM) that contributed to a suite of CMIP5 experiments (Watanabe et al. 2010). In the current study, we use a model version with reduced horizontal resolution of T42 spectral truncation ( $\sim 2.8^\circ$ ) instead of the standard T85 truncation ( $\sim 1.4^\circ$ ). There are 40 hybrid sigma–pressure vertical levels as in the standard T85 setting. Ogura et al. (2017) provided details on the performance of the T42 version of MIROC5-A parameter ensemble. The MIROC5.2-A was updated from Ogura et al. (2017) in that the effect of subgrid snow mass distribution on snow cover by Nitta et al. (2014) and snow-fed wetlands by Nitta et al. (2017) are included in the land surface component, and a diagnostic scheme for ice thickness from observed sea ice concentration is modified to be more realistic. This updated model version is identical to the atmospheric component used in Tatebe et al. (2018). We confirm that the climatological clouds, particularly the vertical profile of tropical mean clouds, are very similar to the ones in Ogura et al. (2017).

HadGEM2-A is the atmospheric component of the HadGEM2-ES AOGCM that contributed to CMIP5 (Jones et al. 2011). The model has 38 levels in the vertical and a horizontal resolution of  $1.25^\circ \times 1.875^\circ$  in latitude and longitude. The model employs geometric height as a vertical coordinate. Further description and performance of the model is given in Martin et al. (2011).

### 3. Method

#### *a. Cloud lifting by FAT mechanism*

In this section we modify the cloud fields from the GCMs to lift the cloud altitude in accordance with what would be predicted by the FAT theory, so that we can quantify the magnitude of the FAT lifting cloud feedback using PRP calculations. According to the FAT theory, the level at which detrainment of the cumulus clouds occurs and the anvil develops is raised as the atmosphere warms, but the temperature of that level remains the same. To mimic this effect on the cloud response, we construct FAT-induced cloud for every radiation time step at every grid point following the method of Lambert et al. (2015): 1) 3-hourly cloud variables (cloud fraction, cloud water amount, and cloud particle size) and air temperature are stored for both control and perturbed experiments and matched up at every time step between the two experiments; 2) the cold points in the vertical are searched for in both experiments above approximately 600 hPa avoiding the surface inversion; and 3) for each grid point, cloud variables at each vertical level between 600 hPa and the cold point are calculated from that level's perturbed temperature by linearly interpolating the cloud variables between

the two control temperatures that bracket the perturbed temperature. The cold point is defined here as the level at which the vertical temperature gradient changes sign. While the choice of 600 hPa as the lower boundary is not definitive, it allows for a smooth vertical profile for high clouds after the interpolation and is loosely consistent with the 680 hPa threshold for the altitude feedback of nonlow clouds adopted by Zelinka et al. (2016). Singh and O'Gorman (2012) also reported that the general response of various atmospheric quantities such as wind speeds, geopotential, temperature, relative humidity, and cloud fraction is captured by an upward shift above 600 hPa. When the perturbed temperature is outside the range of control temperatures in this vertical region, the interpolation for cloud variables is not applied. For those grid points where the interpolation is not applied, control cloud variables are assigned. This procedure is repeated for each atmospheric column. Admittedly this is a very crude way of imitating the FAT response as the FAT theory only states that cloud-top temperature is fixed and not whole cloud temperature, but our method is supported empirically by the multi-GCM analysis of Zelinka and Hartmann (2010, their Figs. 5 and 6). The current procedure results in the upward shift, rather than stretching, of vertical cloud profiles following general tropospheric warming. Nevertheless, it is found that the constructed FAT-induced cloud reproduces the vertical profile of simulated perturbed (AMIP+4K) clouds in the tropical average well as will be shown in section 4a.

#### *b. Partial radiative perturbation analysis*

PRP is a technique to evaluate the radiative effect of changes in individual fields (e.g., water vapor, cloud). This is useful because the total sum of effects from individual fields (evaluated separately) approximately equals the simulated radiation change. It was originally developed by Wetherald and Manabe (1988) and used extensively in many previous studies including Colman (2003) for model ensembles and Yoshimori et al. (2009) for paleoclimate. As is usually the case, this technique is applied to quantify the radiative effect at the TOA in the current study. The diagnosis was made by the following procedure: (i) 3-hourly data that affect the radiative fluxes are stored for both control and perturbed experiments and matched up at every time step between the two experiments, (ii) radiative transfer components of the same AGCMs are used to compute the radiative flux change by changing input variables associated with one feedback component at a time from their control to their perturbed values while holding all others at their control values, (iii) step (ii) is repeated except that input variables are changed from their perturbed to their control values holding all others at their perturbed values, and

(iv) averaging the two. We note that this two-sided analysis was developed by [Colman and McAvaney \(1997\)](#).

The LW cloud feedback due to the simulated clouds (cloud PRP) is, for example, evaluated as follows:

$$\text{cloud PRP} = \frac{1}{2}[R(\mu_0, C_1) - R(\mu_0, C_0) + R(\mu_1, C_1) - R(\mu_1, C_0)], \quad (3)$$

where  $\mu$  represents noncloud variables (specific humidity, temperature, and aerosols), and  $C$  represents cloud variables (i.e., cloud fraction, cloud water amount, and cloud particle size). For HadGEM2-A,  $\mu$  also includes pressure as the model uses a height coordinate. The subscripts 0 and 1 indicate the reference climate (AMIP) and the perturbed climate (AMIP+4K), respectively. The partial radiative effect of the FAT-induced cloud (FAT-cloud PRP) is evaluated by replacing the perturbed clouds ( $C_1$ ) in Eq. (3) by the FAT-induced cloud ( $C_{\text{FAT}}$ ) such that

$$\text{FAT-cloud PRP} = \frac{1}{2}[R(\mu_0, C_{\text{FAT}}) - R(\mu_0, C_0) + R(\mu_1, C_{\text{FAT}}) - R(\mu_1, C_0)]. \quad (4)$$

This PRP calculation moves the cloud to a different altitude following the FAT mechanism (from  $C_0$  to  $C_{\text{FAT}}$ ) but does not change the cloud temperature as a function of height. In other words, cloud temperature is fixed to the original environmental temperature at a given altitude, but the cloud anvil temperature is not fixed as a result of altitude change (as opposed to what the FAT theory predicts).

The cloud masking of each noncloud feedback ( $\alpha \neq \mu'$ ) is given by the difference between all-sky PRP and clear-sky PRP for that feedback such that

$$\begin{aligned} \text{cloud masking of } \alpha &= \frac{1}{2}[R(\alpha_1, \mu'_0, C_0) - R(\alpha_0, \mu'_0, C_0) \\ &\quad - R(\alpha_1, \mu'_0, 0) + R(\alpha_0, \mu'_0, 0)] \\ &\quad + \frac{1}{2}[R(\alpha_1, \mu'_1, C_1) - R(\alpha_0, \mu'_1, C_1) \\ &\quad - R(\alpha_1, \mu'_1, 0) + R(\alpha_0, \mu'_1, 0)] \end{aligned} \quad (5)$$

The total cloud masking of noncloud feedbacks is expressed as

$$\begin{aligned} \text{total cloud masking} &= \frac{1}{2}[R(\mu_1, C_0) - R(\mu_0, C_0) \\ &\quad - R(\mu_1, 0) + R(\mu_0, 0)] \\ &\quad + \frac{1}{2}[R(\mu_1, C_1) - R(\mu_0, C_1) \\ &\quad - R(\mu_1, 0) + R(\mu_0, 0)] \end{aligned} \quad (6)$$

The CRE change is given by

$$\Delta\text{CRE} = R(\mu_1, C_1) - R(\mu_1, 0) - R(\mu_0, C_0) + R(\mu_0, 0), \quad (7)$$

which is equal to the sum of cloud PRP, Eq. (3) and total cloud masking of noncloud feedbacks, Eq. (6). The values for PRP, cloud masking, and  $\Delta\text{CRE}$  are presented in units of  $\text{W m}^{-2} \text{K}^{-1}$  after normalization by the global mean surface air temperature difference between the AMIP+4K and AMIP experiments. Hereafter, we use the terms “cloud PRP” or “FAT-cloud PRP” synonymously with “cloud PRP feedback parameter” or “FAT-cloud PRP feedback parameter,” respectively.

### c. Radiative kernels

Radiative kernels are used to aid the interpretation of the PRP-derived cloud masking effect. We constructed MIROC5.2-A radiative kernels for air temperature, surface temperature, and water vapor following the procedure described by [Soden et al. \(2008\)](#). These consist of both all-sky and clear-sky components of TOA radiation anomalies in response to unit increases in air temperature and surface temperature, and to specific humidity changes expected from unit air temperature increases under the fixed relative humidity assumption. They are constructed separately for each variable, and the specific humidity and air temperature are perturbed at each model vertical level separately. The kernels are then scaled by the simulated changes between AMIP+4K and AMIP in those variables on the native model vertical coordinate to estimate their contributions to the TOA radiation change. The cloud masking of each feedback is then obtained by subtracting the clear-sky component from the all-sky component for each feedback. In addition to these standard kernels for “warming perturbation” with respect to AMIP, we constructed those for “cooling perturbation,” that is, unit decrease, instead of unit increase, in the above perturbations with respect to AMIP+4K to investigate the sensitivity of cloud masking to a different background climatology. All radiative kernels are monthly averaged from a 1-yr integration run using AMIP forcings for 1979.

## 4. Results

### a. Radiative feedback of clouds lifted by the FAT mechanism

[Figure 2](#) shows tropical and annual mean vertical profiles of air temperature and cloud fraction above 700 hPa. The tropopause is located near 100 hPa in both experiments for MIROC5.2-A and HadGEM2-A. The maximum high cloud fractions of about 0.09 and 0.13 are

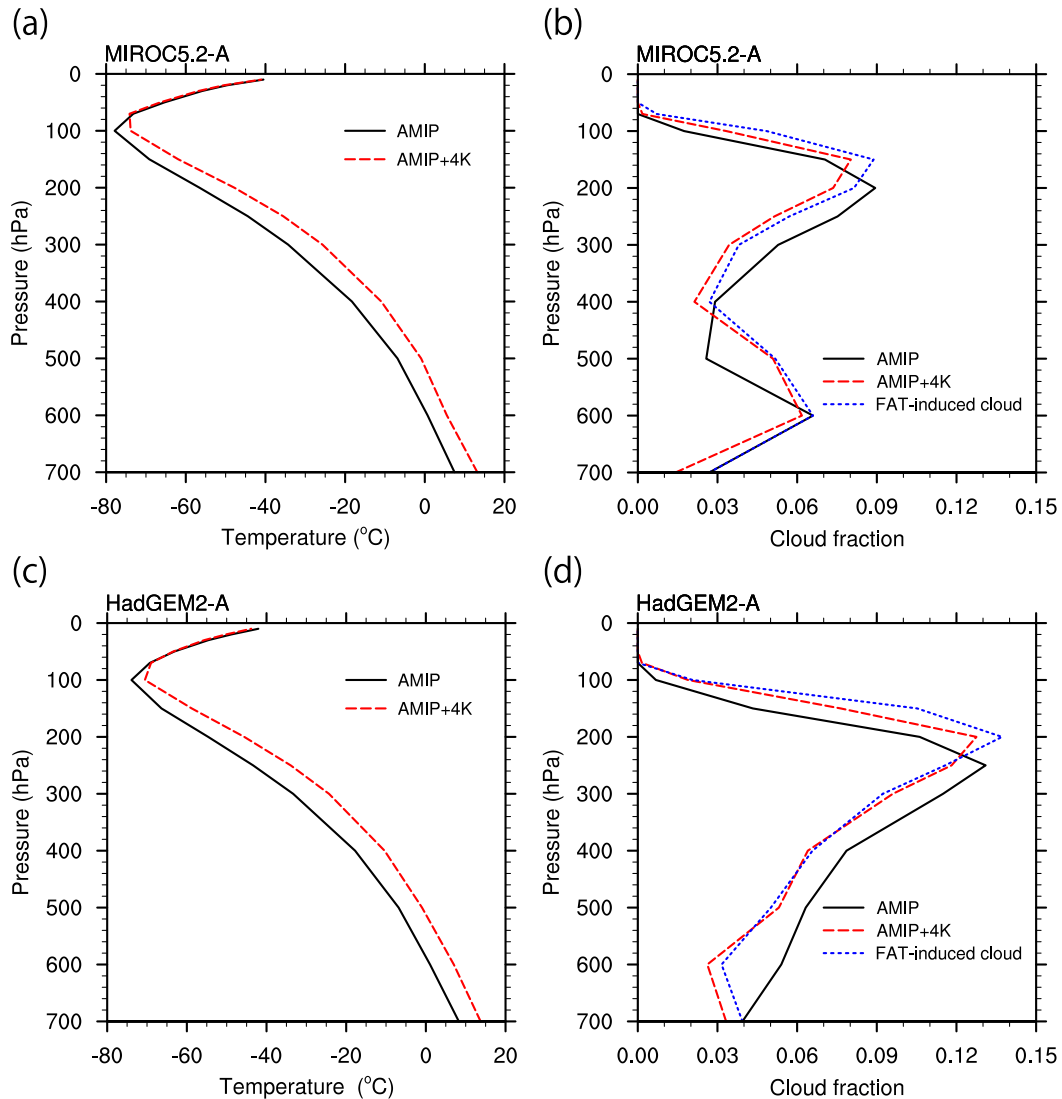


FIG. 2. Vertical profiles of annual mean fields averaged over the tropical region ( $30^{\circ}\text{S}$ – $30^{\circ}\text{N}$ ) in the AMIP and AMIP+4K experiments: (a) MIROC5.2-A temperature ( $^{\circ}\text{C}$ ); (b) MIROC5.2-A cloud fraction; (c) HadGEM2-A temperature ( $^{\circ}\text{C}$ ); and (d) HadGEM2-A cloud fraction. FAT-induced cloud is also plotted in (b) and (d).

located near 200 and 250 hPa for MIROC5.2-A and HadGEM2-A, respectively, in the AMIP experiment. The cloud fraction in *CALIPSO* simulator output from the AMIP experiment is compared with satellite-derived data [*CALIPSO*–GCM-Oriented Cloud Product (GOCCP) 2007–16 average, not shown] (Chepfer et al. 2010). In the tropical average, both models overestimate the local maximum cloud fraction in the upper troposphere in which MIROC5.2-A and HadGEM2-A show about 9% (at 13 km in altitude) and about 12% (at 11 km), respectively, whereas *CALIPSO*–GOCCP shows only about 6% (at 13 km). MIROC5.2-A has a distinct local maximum cloud fraction of about 8% in the midtroposphere (at 4 km) that is absent in HadGEM2-A but that may

correspond to broad peaks in the cloud fraction of about 3% (at 5–7 km) in *CALIPSO*–GOCCP.

The vertical profiles of clouds generally shift upward, and the levels of maximum cloud fraction are elevated to about 150 and 200 hPa for MIROC5.2-A and HadGEM2-A, respectively, in the AMIP+4K experiments. In both models, the maximum cloud fraction in the AMIP+4K becomes smaller than the AMIP. The reduction of cloud amount is a robust feature in GCMs (Zelinka and Hartmann 2010) and a hierarchy of atmospheric models (Bony et al. 2016) and a potential explanation was already provided by Zelinka and Hartmann (2010): an increase of static stability requires a smaller rate of subsidence in order

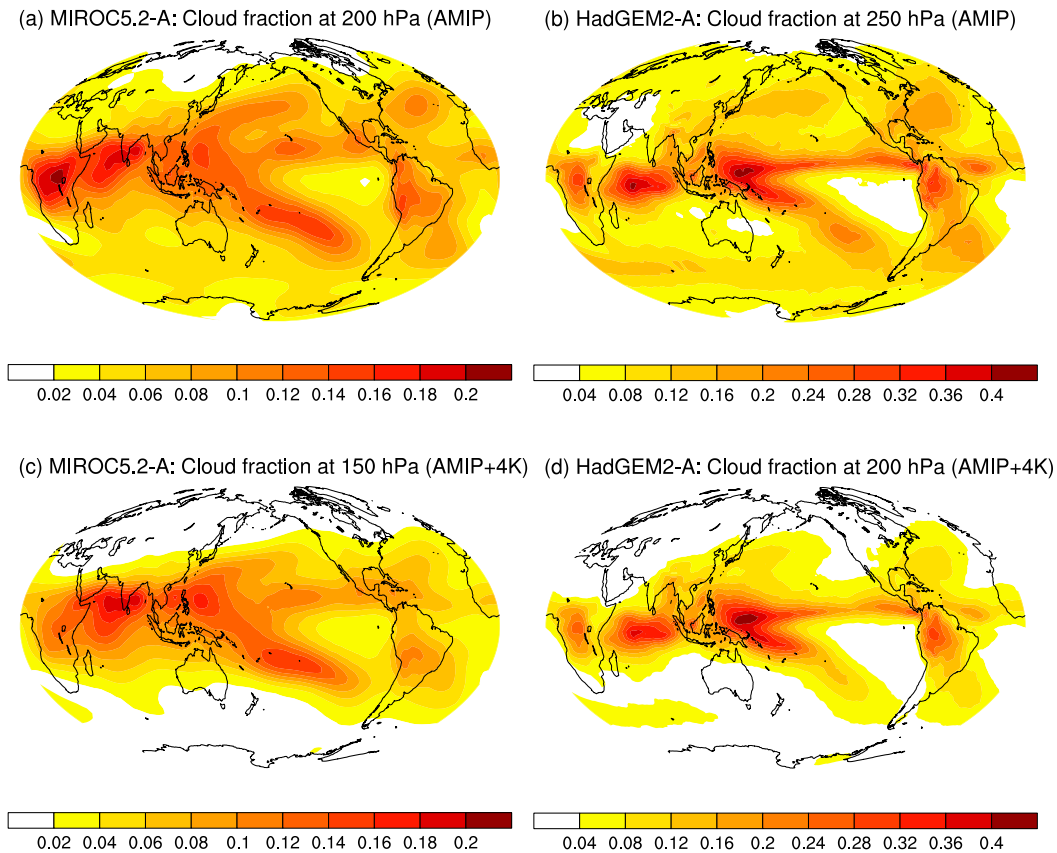


FIG. 3. Cloud fraction (a) MIROC5.2-A at 200 hPa in the AMIP experiment; (b) MIROC5.2-A at 150 hPa in the AMIP+4K experiment; (c) HadGEM2-A at 250 hPa in the AMIP experiment; and (d) HadGEM2-A at 200 hPa in the AMIP+4K experiment. Note that color scales are different for (left) MIROC5.2-A and (right) HadGEM2-A.

to balance the same radiative cooling in the clear-sky region. We note, however, that cases of high cloud amount increase with raised SST in a cloud-resolving model were also reported (Ohno and Satoh 2018). In Figs. 2b and 2d, the FAT-induced cloud is also plotted, and it captures the upward shift of the AMIP+4K clouds well without reducing the amount of cloud in the upper troposphere. The horizontal distribution of high clouds at the level of maximum cloud fraction is shown in Figs. 3a and 3b for the AMIP and Figs. 3c and 3d for the AMIP+4K. The HadGEM2-A cloud fraction tends to have sharper geographic peaks than MIROC5.2-A, which enables us to sample different background cloud distributions.

In the PRP framework, the cloud feedback is evaluated by replacing the background clouds with the clouds simulated in the perturbed experiment (cloud PRP). Figures 4a and 4b show the cloud PRP components for MIROC5.2-A and HadGEM2-A, respectively. The (LW) cloud PRP feedbacks are  $0.16 \text{ W m}^{-2} \text{ K}^{-1}$  for MIROC5.2-A and  $0.81 \text{ W m}^{-2} \text{ K}^{-1}$  for HadGEM2-A in the tropical

average (Tables 1 and 2). The value for HadGEM2-A appears within the range of 12 models presented in Fig. 12a of Zelinka and Hartmann (2010) but the value for MIROC5.2-A is at the lower end. There are regions of positive and negative values. Positive values prevail in the western Pacific warm pool region, South Pacific convergence zone, large parts of the Indian Ocean, and near Mexico while large negative values occur in equatorial Africa for both models. In general, (LW) FAT-cloud PRP is expected to be positive as the level of maximum cloud fraction moves upward where the environmental temperature is lower in the background. Indeed, both MIROC5.2-A and HadGEM2-A yield positive values in the tropical and global averages (Table 3). The (LW) FAT-cloud PRP feedbacks are  $0.26 \text{ W m}^{-2} \text{ K}^{-1}$  for MIROC5.2-A and  $0.62 \text{ W m}^{-2} \text{ K}^{-1}$  for HadGEM2-A in the tropical average. The level of agreement between cloud PRP and FAT-cloud PRP is comparable with Zelinka and Hartmann (2010). While the spatial distribution of FAT-cloud PRP (Figs. 4c,d) is different from that of cloud PRP, the cloud feedback induced by the



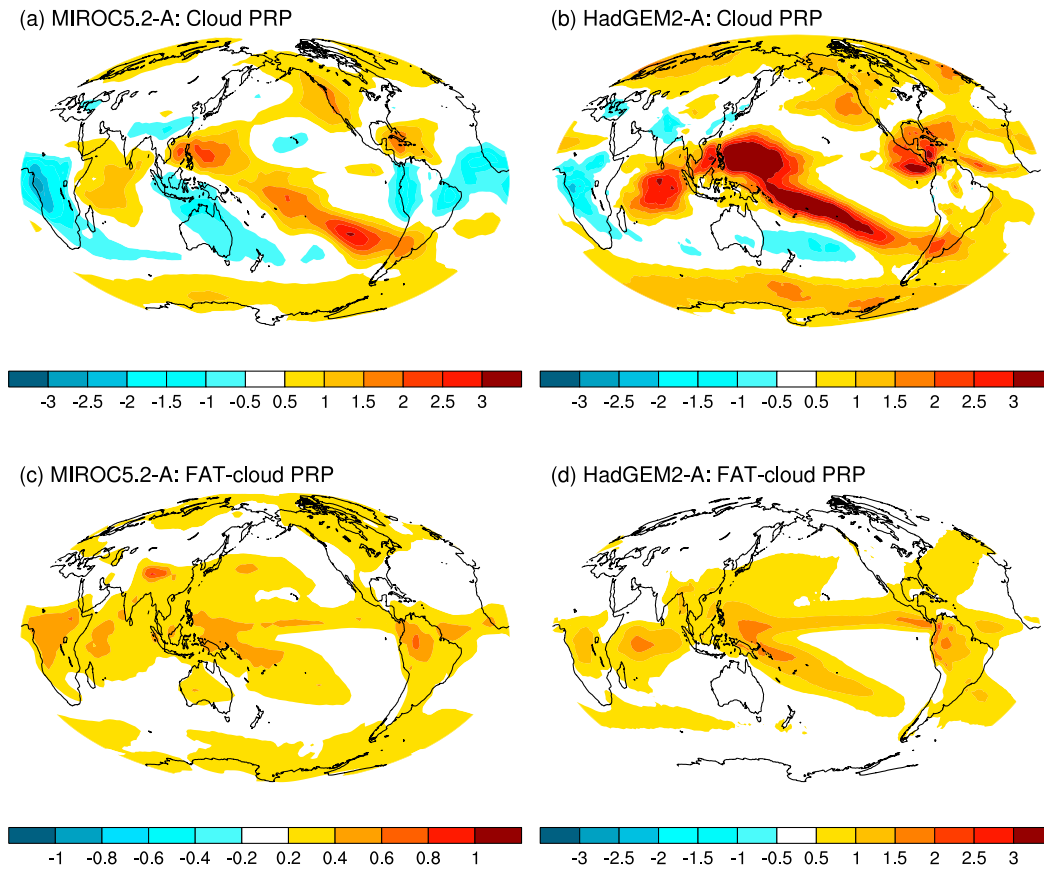


FIG. 4. LW component of the PRP analysis ( $\text{W m}^{-2} \text{K}^{-1}$ ): (left) MIROC5.2-A and (right) HadGEM2-A; (a),(b) simulated clouds and (c),(d) FAT-induced cloud. Note that the color scale in (c) is different from others.

FAT mechanism is positive through the “cloud altitude effect” in the PRP framework.

*b. A new framework for the thermal radiative damping and “residual” cloud feedback*

As stated in the introduction, Held and Shell (2012) proposed to treat the RH, rather than the specific humidity,

as a state variable in PRP-type feedback analysis. One of their motives was the fact that the change of temperature or specific humidity alone is not “recognizable” in nature. Broadly speaking, RH in GCMs does not change much with climate although there are of course regional exceptions (Sherwood et al. 2010). The amount of water vapor under the fixed RH constraint is determined solely by the

TABLE 1. Standard PRP result for the MIROC5.2-A model. “Residual” denotes the difference between the sum of all PRP terms and simulated TOA net radiation change. Lapse rate feedback is diagnosed by the difference between (total) temperature and Planck feedback. Units are in  $\text{W m}^{-2} \text{K}^{-1}$  unless indicated explicitly (i.e., %). “Masking” represents the difference between all-sky and clear-sky components and is expressed both in  $\text{W m}^{-2} \text{K}^{-1}$  and as a fraction of all-sky feedback that is masked by clouds in units of %. Percentage for the cloud masking is not shown when the all-sky component is less than  $0.1 \text{ W m}^{-2} \text{K}^{-1}$ .

	Global				Tropics			
	All sky	Clear sky	Masking	Masking (%)	All sky	Clear sky	Masking	Masking (%)
Water vapor	1.70	2.31	−0.61	−35.9	2.30	3.10	−0.80	−34.8
Cloud	0.25	—	—	—	0.16	—	—	—
Aerosol	0.00	0.00	0.00	—	0.00	0.00	0.00	—
Temperature	−4.06	−4.31	0.25	−6.2	−4.60	−4.84	0.23	−5.0
Planck	−3.60	−3.91	0.31	−8.7	−3.71	−4.06	0.35	−9.5
Lapse rate	−0.46	−0.40	−0.06	13.4	−0.89	−0.78	−0.12	13.3
PRP total	−2.11	−2.00	−0.36	—	−2.14	−1.73	−0.57	—
Simulation	−2.10	−2.00	—	—	−2.13	−1.72	—	—
Residual	−0.01	0.00	—	—	−0.01	−0.01	—	—

TABLE 2. As in Table 1, but for HadGEM2-A with a pressure term (see text for details). Unlike MIROC5.2-A in Table 1, the lapse rate feedback is computed explicitly.

	Global				Tropics			
	All sky	Clear sky	Masking	Masking (%)	All sky	Clear sky	Masking	Masking (%)
Water vapor	2.09	2.87	-0.78	-37.3	2.85	3.79	-0.94	-33.1
Cloud	0.72	—	—	—	0.81	—	—	—
Aerosol	0.01	0.02	-0.01	—	0.02	0.02	-0.01	—
Temperature	-3.89	-4.00	0.11	-2.8	-4.52	-4.53	0.01	-0.1
Planck	-3.88	-4.08	0.20	-5.1	-4.15	-4.30	0.15	-3.7
Lapse rate	-0.09	0.09	-0.17	—	-0.51	-0.23	-0.28	55.5
Pressure	-1.05	-0.82	-0.23	21.6	-1.23	-0.99	-0.24	19.6
PRP total	-2.19	-1.92	-0.90	—	-2.22	-1.71	-1.18	—
Simulation	-1.85	-1.93	—	—	-1.72	-1.70	—	—
Residual	-0.34	0.01	—	—	-0.49	0.00	—	—

temperature. The majority of conventional water vapor feedback that does not contribute to the total feedback due to the anticorrelation with the lapse rate feedback is absorbed into the “temperature + fixed RH” component of the feedback in the Held–Shell framework. It then becomes the RH response that needs to be understood in order to constrain the total feedback.

We propose a new LW feedback framework, thermal radiative damping with fixed relative humidity and anvil temperature (T-FRAT), by rearranging the conventional feedback decomposition. The T-FRAT feedback consists of temperature, specific humidity predicted by the fixed RH assumption, and clouds predicted by the fixed temperature–cloud relation (i.e., FAT-induced cloud). It only includes the LW components. This rearrangement is an extension of the Held–Shell framework that now adds a FAT theory component. In Fig. 5a, the conventional decomposition of temperature ( $\Lambda_T$ ) and water vapor (specific humidity) ( $\Lambda_q$ ) feedbacks are shown in the left two columns, and the Held–Shell fixed RH temperature feedback ( $\tilde{\Lambda}_{T-FR}$ ) and RH feedback ( $\tilde{\Lambda}_{RH}$ ) are shown in the right two columns for the two models. The basic physical response component under fixed RH assumption ( $\tilde{\Lambda}_{T-FR}$ ) constitutes a single feedback, and the RH feedback (or “residual” water vapor feedback) are located near the zero line. In Fig. 5b, the conventional decomposition of temperature, water vapor, and cloud ( $\Lambda_C$ ) feedbacks are shown in the left three columns, and the new decomposition proposed in the current study is shown in the right three columns, including the T-FRAT component ( $\tilde{\Lambda}_{T-FRAT}$ ). The basic physical response component under fixed RH and anvil temperature assumptions constitutes a single feedback, and the residual water vapor feedback and non-FAT component of cloud feedback (or “residual cloud feedback”) ( $\tilde{\Lambda}_C$ ) are located near the zero line. The residual cloud feedback represents the sum of LW components of the low ( $p > 600$  hPa) cloud feedback, the nonlow

( $p < 600$  hPa) amount and optical depth feedbacks, nonlow deviations-from-FAT altitude feedback, and their interactions. The cancellation between temperature and cloud feedbacks (as well as between temperature and water vapor feedbacks) in the conventional decomposition are reduced. It is now the non-fixed-RH component of water vapor feedback and the non-FAT component of cloud feedback that need to be understood in order to constrain the total feedback.

One of the aims of the new framework is to combine cancelling feedbacks and highlight feedbacks that contribute to the total feedback. As discussed in section 4a, FAT–cloud PRP represents most of the high cloud altitude feedback, which is expected to be larger if more warming occurs at higher altitudes. Therefore, it is of interest to investigate the sensitivity of the FAT–cloud PRP to the magnitude of lapse rate feedback. This sensitivity is tested for MIROC5.2-A by halving the departures of temperature profile from the vertically uniform temperature change that is equal to the magnitude of surface temperature change ( $\Delta LR \times 0.5$ ). Cases for even more reduced lapse rate responses of one quarter ( $\Delta LR \times 0.25$ ) and zero (i.e., Planck response,  $\Delta LR \times 0$ ) were carried out for 5 years (1979–83). The 30-yr averages are not significantly different from the 5-yr averages for  $\Delta LR \times 1$  (AMIP+4K) and  $\Delta LR \times 0.5$  (Table 4). Figure 6a shows the anomalous temperature profiles for the different cases of lapse rate change from

TABLE 3. PRP feedback and change in cloud radiative effect for FAT-induced cloud ( $W m^{-2} K^{-1}$ ).

	MIROC5.2-A		HadGEM2-A	
	Global	Tropics	Global	Tropics
Cloud PRP	0.25	0.16	0.72	0.81
FAT–cloud PRP	0.22	0.26	0.49	0.62
Cloud masking	-0.36	-0.57	-0.90	-1.18
FAT–cloud $\Delta CRE$	-0.14	-0.31	-0.40	-0.56

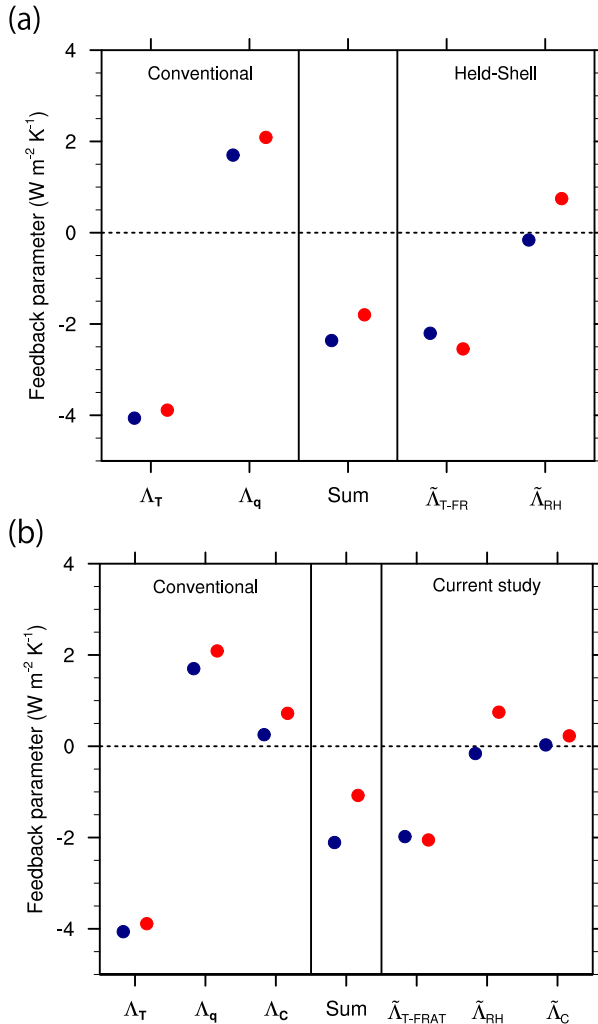


FIG. 5. Feedback parameters with different decompositions. (a) Held-Shell framework: (left two columns) conventional temperature ( $\Lambda_T$ ) and water vapor ( $\Lambda_q$ ) feedbacks; (right two columns) Held-Shell decomposition of thermal radiative damping with fixed RH ( $\tilde{\Lambda}_{T-FR}$ ) and  $\Delta$ RH ( $\tilde{\Lambda}_{RH}$ ) feedbacks, respectively; and (middle column) the sum. (b) New framework proposed in the current study: (left three columns) conventional temperature, water vapor, and cloud ( $\Lambda_C$ ) feedbacks; (right three columns) T-FRAT ( $\tilde{\Lambda}_{T-FRAT}$ ),  $\Delta$ RH, and residual (non-FAT) cloud ( $\tilde{\Lambda}_C$ ) feedbacks, respectively; and (middle column) the sum. Navy circles are for MIROC5.2-A and red circles for HadGEM2-A. Note that the sums in (a) and (b) are different.

the AMIP experiment. While we also perturbed stratospheric temperature for simplicity, it should not have much effect as little water vapor and clouds exist there. Figure 6b shows the specific humidity profiles under the assumption of fixed RH for different cases of lapse rate change. The fixed-RH water vapor feedback decreases when the lapse rate feedback increases, keeping the sum of the two feedbacks nearly constant (Table 4). Figures 6c and 6d show the same but for the FAT-induced cloud and

anomalous FAT-induced cloud with respect to the AMIP experiment, respectively. Although a smaller increase of the cloud altitude is noticeable between 400 and 200 hPa in Fig. 6c when the lapse rate response is halved, the pressure level of maximum cloud fraction at about 150–200 hPa does not change much between the original and halved lapse rate response cases. It is thus expected that the difference in cloud altitude feedback is small. Indeed, the impact of lapse rate difference for FAT-cloud PRP is very small while the lapse rate and fixed-RH water vapor feedback change substantially (Table 4). In contrast, two additional experiments of  $\Delta$ LR $\times$ 0.25 and  $\Delta$ LR $\times$ 0 show distinctly smaller increases of cloud fraction between 150 and 100 hPa (Fig. 6d), and smaller FAT-cloud PRP (Table 4 and Fig. 7) relative to  $\Delta$ LR $\times$ 1. Collectively, the result of sensitivity experiments shows that there is some degree of cancellation between the lapse rate feedback and FAT-cloud PRP, and the range of the combined term is smaller compared to the range of the lapse rate feedback (Table 4 and Fig. 7).

However, the negative Planck-induced FAT-cloud PRP requires some discussion. The result is explained by the disappearance of unperturbed clouds just below the tropopause, because the unperturbed clouds cannot rise further under warming since the tropopause level (defined here by the cold point) does not change in altitude with the Planck response, that is, vertically uniform warming. This result raises the following conceptual issue. While the combination of temperature feedback and FAT-cloud feedback into a single term does make physical sense as the tropopause rises with the tropospheric warming, the combination of Planck-derived cloud lifting and constant tropopause height does not. However, this situation is unlikely to occur in nature. Therefore, the decomposition of temperature feedback into Planck and lapse rate feedbacks may not be useful to apply within the T-FRAT framework, and the cancellation between the extra warming in the upper troposphere (negative lapse rate feedback) and the FAT-cloud PRP shown in Table 4 is likely overestimated. This result is not necessarily encouraging, but it reminds us that the lapse rate change contains two components: upper-tropospheric warming and tropopause rise. A further refinement of our method in constructing FAT-induced cloud profiles from the control clouds may be worth exploring in the future as discussed in section 5.

### c. Interpretation of cloud masking effects and their implications for the change in cloud radiative effect

It is useful to refine the interpretation of cloud masking before  $\Delta$ CRE, the sum of cloud PRP and cloud masking, is discussed. The cloud masking effects on noncloud feedbacks were previously described by Soden

TABLE 4. PRP result of (all sky) lapse rate feedback, water vapor feedback under the fixed-RH assumption, and FAT–cloud feedback for MIROC5.2-A ( $\text{W m}^{-2} \text{K}^{-1}$ ). Results for 5-yr average (1979–83) are presented except for “ $\Delta\text{LR}\times 1$ ” and “ $\Delta\text{LR}\times 0.5$ ” in which 30-yr average (1979–2008) are also presented in brackets. “ $\Delta\text{LR}\times 1$ ” denotes the case in which the simulated lapse rate change (AMIP+4 K – AMIP) is used. “ $\Delta\text{LR}\times 0.5$ ,” “ $\Delta\text{LR}\times 0.25$ ,” and “ $\Delta\text{LR}\times 0$ ” denote the cases in which the lapse rate response was reduced to one-half, one quarter, and zero, respectively.

	Global			Tropics		
	Lapse rate	Water vapor	FAT-induced cloud	Lapse rate	Water vapor	FAT-induced cloud
$\Delta\text{LR}\times 1$	–0.48 (–0.46)	1.87 (1.86)	0.23 (0.22)	–0.89 (–0.89)	2.52 (2.50)	0.26 (0.26)
$\Delta\text{LR}\times 0.5$	–0.20 (–0.19)	1.52 (1.51)	0.22 (0.22)	–0.42 (–0.42)	2.02 (2.00)	0.26 (0.26)
$\Delta\text{LR}\times 0.25$	–0.09	1.37	0.10	–0.20	1.79	0.08
$\Delta\text{LR}\times 0$	0.00	1.23	–0.04	0.00	1.57	–0.09

et al. (2008). Here we restrict our discussion to the LW component, and further decompose the cloud masking effect on the temperature feedback into Planck and lapse rate components. Negative cloud masking means that the presence of clouds reduces a positive noncloud feedback or enhances a negative noncloud feedback. Conversely, positive cloud masking means that the presence of clouds reduces a negative noncloud feedback or enhances a positive noncloud feedback.

Figure 8 shows the cloud masking of the water vapor, Planck, lapse rate, and temperature feedbacks (i.e., the sum of Planck and lapse rate components) for the MIROC5.2-A and HadGEM2-A. These are obtained by subtracting the clear-sky version of each PRP feedback term (calculated with no clouds) from the all-sky version [Eq. (5)]. Their global and tropical mean values are summarized in Tables 1 and 2. In addition, the contribution to the TOA cloud masking from each vertical level is diagnosed for MIROC5.2-A using the radiative kernels constructed with the AMIP background climatology in section 3c. Figure 9 shows the result for the tropical average. The vertical integrations of Fig. 9 approximately yield the tropical mean values for MIROC5.2-A in Fig. 8, meaning that the kernel analysis in Fig. 9 helps us interpret the PRP-derived vertically integrated picture of Fig. 8 with vertical resolution.

As the LW water vapor feedback is positive, meaning that an increase of water vapor under warming reduces the clear-sky OLR, the presence of high clouds above the clear-sky emitting level is expected to reduce the magnitude of water vapor feedback. Consistent with this expectation, Figs. 8a and 8b show negative values in all geographical regions, and Fig. 9 shows that the contribution to the cloud masking of the water vapor feedback is negative throughout the troposphere.

In contrast, the Planck response is negative (Tables 1 and 2) and the cloud masking of the Planck response is positive (Figs. 8c,d). Compared with the clear-sky case, the presence of high clouds raises the effective emission

level to colder temperatures, where an increase in temperature is less effective at increasing OLR. The spatial pattern of the masking primarily reflects the cloud distribution at 200 hPa (Fig. 3a) where high cloud cover is maximum (Fig. 2b) for MIROC5.2-A, and Fig. 9 shows that high clouds around 200 hPa contribute negatively to the cloud masking. The contribution from the surface is opposite in sign to that from the three tropospheric levels (~200, 600, and 850 hPa) where the vertical profile of cloud fraction has local peaks in the tropical average. The total atmospheric contribution adds up to be negative ( $-0.03 \text{ W m}^{-2} \text{ K}^{-1}$ ), but the larger contribution from the surface ( $0.39 \text{ W m}^{-2} \text{ K}^{-1}$ ) makes the cloud masking of the Planck response positive.

The sign of the cloud masking effect on the lapse rate feedback is not obvious prior to a proper diagnosis. Compared with the clear-sky case, the presence of high clouds raises the effective emission level to higher, colder levels where larger warming occurs in the tropics between AMIP+4K and AMIP. However, although the lowering of emission temperature leads to positive cloud masking, the larger warming that occurs at higher altitudes leads to negative cloud masking. Figures 8e and 8f show that the cloud masking of the lapse rate feedback is negative, and Fig. 9 indicates that it is due to the OLR increase from high clouds where a large warming occurs for MIROC5.2-A. The cloud masking of the temperature feedback is negative in parts of the Southern Hemisphere subtropics where surface warming is small, but the warming aloft is large due to the constraint of the weak thermal gradient in the tropical and subtropical free-troposphere (Fig. 8g). Similar constraints determine geographical differences in the lapse rate feedback itself, as discussed by Lambert and Taylor (2014) and Ferraro et al. (2015). The negative values in cloud masking of lapse rate feedback are more pronounced in HadGEM2-A (Fig. 8f), which is responsible for the prevailing negative cloud masking of temperature feedback (Fig. 8h) despite the positive cloud masking of Planck response (Fig. 8d). Therefore, the cloud masking

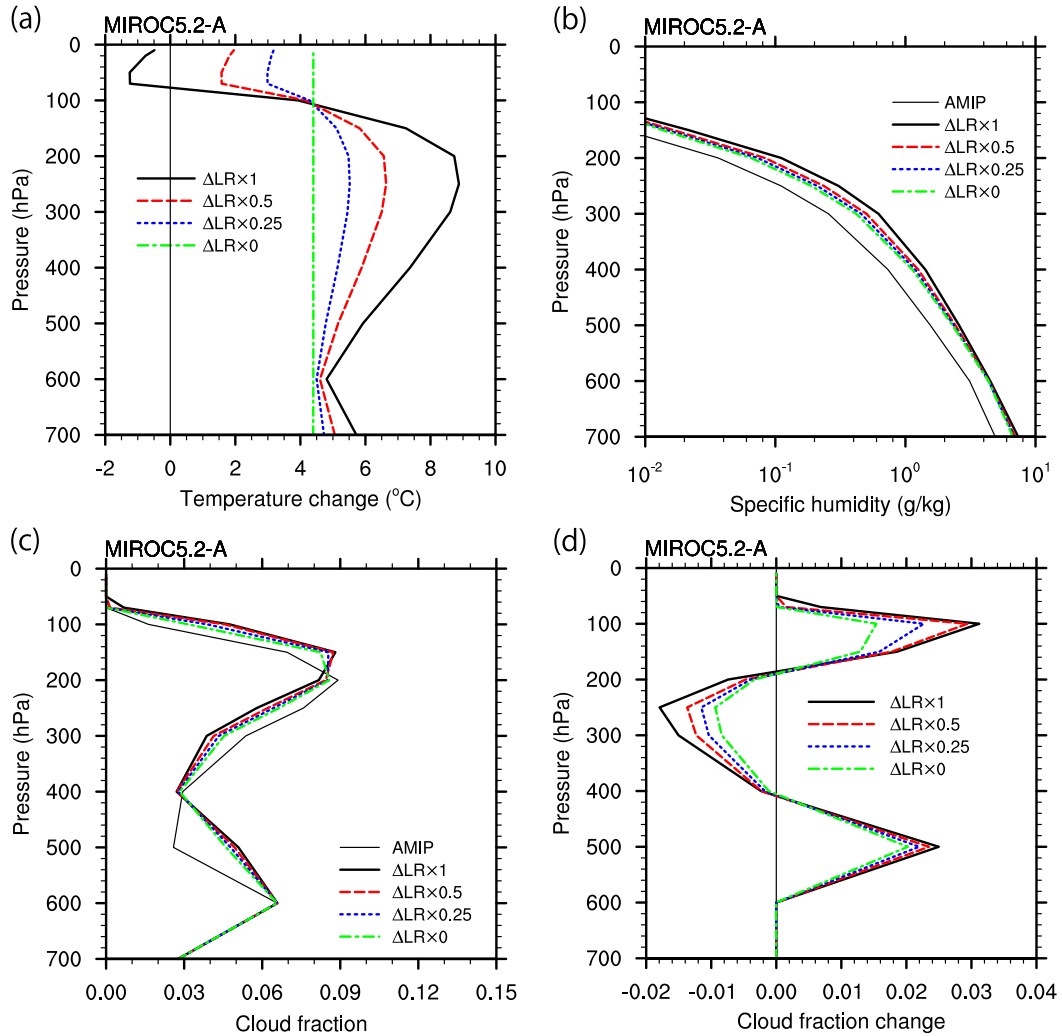


FIG. 6. Vertical profiles of annual mean fields averaged over the tropical region ( $30^{\circ}\text{S}$ – $30^{\circ}\text{N}$ ) for (a) air temperature difference from the AMIP run; (b) specific humidity; (c) cloud fraction; and (d) cloud fraction difference from the AMIP run. “ $\Delta LR \times 1$ ” denotes the case in which the simulated lapse rate change (AMIP+4K – AMIP) is used. “ $\Delta LR \times 0.5$ ,” “ $\Delta LR \times 0.25$ ,” and “ $\Delta LR \times 0$ ” denote the cases in which the lapse rate response was reduced to one-half, one quarter, and zero, respectively. Results for 5-yr average (1979–83) are presented.

of the temperature feedback is not necessarily positive, and the tropical mean value for HadGEM2-A is neutral (Table 2).

These results suggest that the cloud masking effect is more universally understood in terms of changes in the effective emission level, rather than the interruption of upwelling LW radiation compared to the clear-sky case. The term “cloud masking effect,” thus, may be more precisely described as “impact of climatological clouds on noncloud feedbacks” or “cloud climatology effect” for short, which may mask feedbacks (weakening their magnitude) in some cases but enhance them in others. In particular, the lapse rate plays a role in determining the sign of the cloud masking of the temperature feedback.

An illustration summarizing the impact of climatological clouds on noncloud feedbacks is given in Fig. 10.

Figure 11 shows  $\Delta CRE$  for FAT-induced cloud constructed by the sum of FAT-cloud PRP [Eq. (4)] and the cloud masking of temperature and water vapor feedbacks computed with the two-sided PRP [Eq. (5)]. While the sum of FAT-cloud PRP and the cloud masking of temperature feedback alone is positive except for small regions in the southeastern tropical Pacific and Atlantic (Figs. 11a,b), the large negative cloud masking of water vapor feedback makes  $\Delta CRE$  negative over large part of the tropical oceans (Figs. 11c,d, Table 3). As  $\Delta CRE$  is an observable quantity in contrast to cloud PRP, it is important to understand these

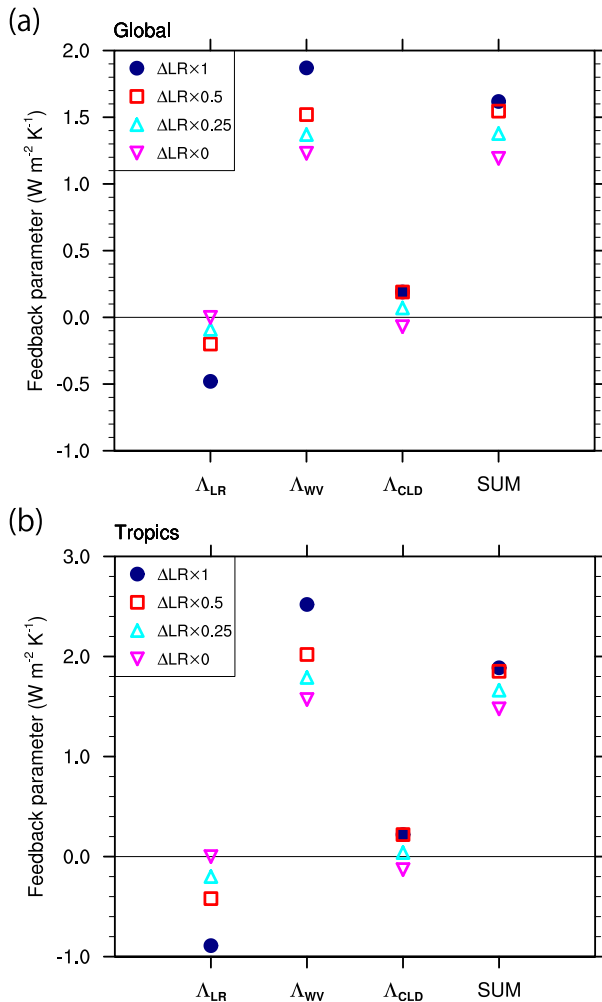


FIG. 7. Sensitivity of fixed-RH water vapor ( $\Delta_{\text{WV}}$ ) and FAT-cloud ( $\Delta_{\text{CLD}}$ ) feedback parameters to different lapse rate feedbacks ( $\Delta_{\text{LR}}$ ): (a) global average; and (b) tropical average. “ $\Delta_{\text{LR}} \times 1$ ” denotes the case in which the simulated lapse rate change (AMIP+4K – AMIP) is used. “ $\Delta_{\text{LR}} \times 0.5$ ,” “ $\Delta_{\text{LR}} \times 0.25$ ,” and “ $\Delta_{\text{LR}} \times 0$ ” denote the cases in which the lapse rate response was reduced to one-half, one quarter, and zero, respectively. Results for 5-yr average (1979–83) are presented, and their numerical values are given in Table 4.

masking effects to constrain the FAT-cloud radiative effect in observations. They are currently model dependent.

Strictly speaking, the cloud masking computed by two-sided PRP contains not only the effect of AMIP cloud but also of AMIP+4K cloud. The latter effect should be irrelevant to the  $\Delta_{\text{CRE}}$  for FAT-induced cloud. We checked the sensitivity of cloud masking to the different cloud climatology of AMIP and AMIP+4K for MIROC5.2-A using the radiative kernels constructed with AMIP cloud (warming perturbation in section 3c) and with AMIP+4K cloud (cooling perturbation in section 3c), separately. Table 5 summarizes the results. The difference in cloud masking between the two-sided PRP and the radiative

kernel with AMIP cloud is smaller than  $0.05 \text{ W m}^{-2} \text{ K}^{-1}$  for both water vapor and temperature feedbacks. Although the results differ quantitatively, the qualitative conclusion for  $\Delta_{\text{CRE}}$  does not depend on which cloud masking is used.

## 5. Discussion

There are two different ways of understanding the FAT effect on climate feedbacks, which are associated with the different approaches for decomposing feedbacks and diagnosing cloud radiative feedback parameters discussed in the introduction. As in Eq. (2), the LW cloud feedback parameter is defined by  $\Lambda_C = \partial R / \partial C \cdot dC/dT_s$ . The zero-cloud-emission-change feedback derived from the FAT mechanism accompanies constant cloud anvil temperature, which implies  $dC/dT_s = 0$  with  $C$  being the cloud temperature, and hence  $\Lambda_C = 0$ , that is, a zero cloud feedback parameter. The FAT-cloud PRP, on the other hand, includes the effect of cloud anvil temperature change to colder temperatures at higher altitude allowing for  $dC/dT_s \neq 0$ , and hence a nonzero cloud feedback parameter. In these two different radiative decompositions, therefore,  $\Lambda_C$  refers to different quantities. A similar argument applies to  $\Lambda_T$ , and the difference in  $\Lambda_C$  is offset by the difference in  $\Lambda_T$  between the two alternative decompositions (Figs. 1b,c). This understanding motivated us to propose the T-FRAT framework, in which the cloud feedback parameter for the zero-cloud-emission-change feedback is, by definition, zero.

We argue that part of the opposing effects of conventional thermal radiative damping and FAT-cloud PRP feedback is caused by the cancellation between the cloud emission component of the temperature feedback and the cloud altitude feedback. The temperature feedback also contains a component arising from the interception of upwelling LW radiation by climatological clouds, but this component is not cancelled by the cloud altitude feedback. For example, suppose we have two extreme cases of 0% and 100% high cloud fraction with the 100% case moving upward in accordance with FAT in response to a general warming. For the 100% cloud cover case, we expect that the cloud emission component of the temperature feedback through the increase in temperature at a given level will be nearly cancelled by the cloud altitude feedback through the decrease of cloud anvil temperature. If the cloud masking of the temperature feedback is positive, however, a smaller negative temperature feedback in the 100% cloud cover case is expected compared to the 0% cloud cover case. Therefore, the cancellation of the temperature feedback by the FAT-cloud feedback is partial, and consequently the degree of cancellation between the conventional thermal radiative damping and the FAT-cloud feedback may depend on the GCM.

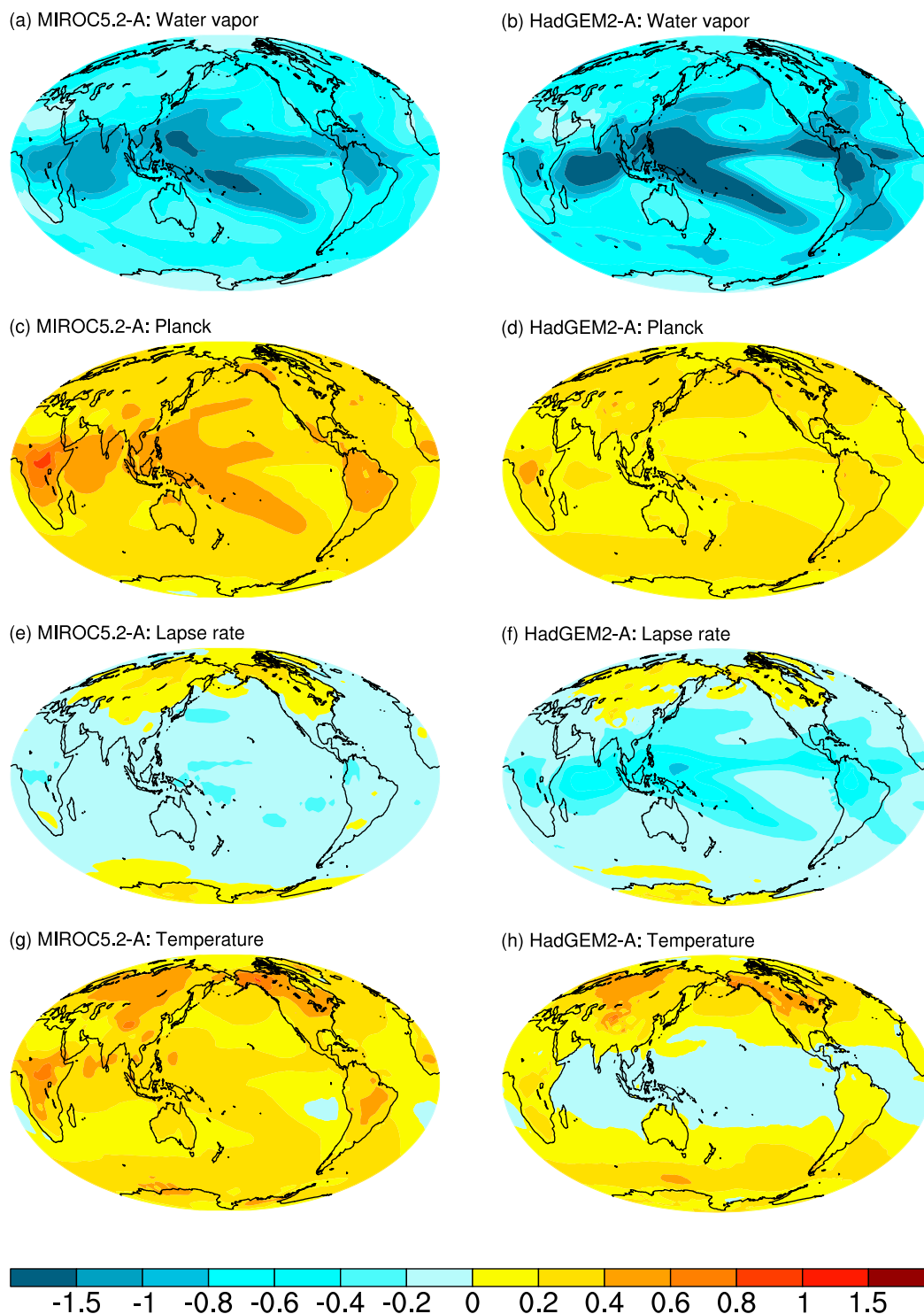


FIG. 8. Cloud masking of LW feedbacks ( $\text{W m}^{-2} \text{K}^{-1}$ ): (left) MIROC5.2-A and (right) HadGEM2-A; (a),(b) water vapor, (c),(d) Planck, (e),(f) lapse rate, and (g),(h) temperature (Planck + lapse rate). As defined in the text, positive cloud masking means that the presence of clouds reduces a negative noncloud feedback or enhances a positive noncloud feedback.

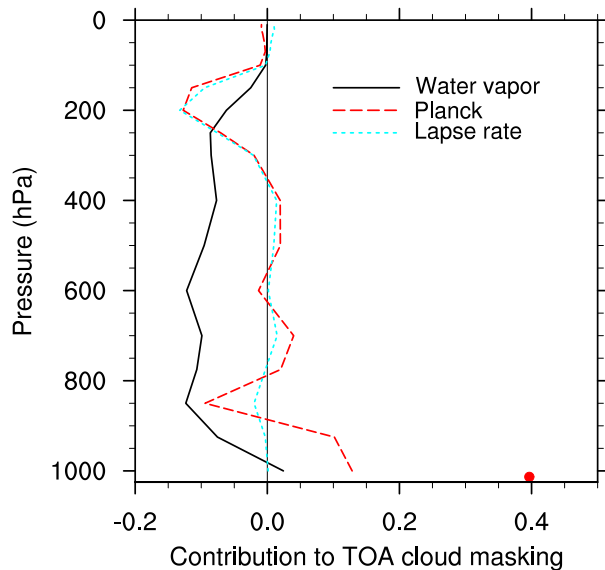


FIG. 9. Contribution to the TOA cloud masking from individual vertical levels averaged over the tropical region ( $30^{\circ}\text{S}$ – $30^{\circ}\text{N}$ ) for MIROC5.2-A. Values are normalized by 100 hPa layer thickness for the atmosphere [ $\text{W m}^{-2}\text{K}^{-1}$  ( $100\text{ hPa})^{-1}$ ]. For the cloud masking of Planck response, the surface contribution is also plotted at the bottom ( $\text{W m}^{-2}\text{K}^{-1}$ ). As defined in the text, positive cloud masking means that the presence of clouds reduces a negative noncloud feedback or enhances a positive noncloud feedback.

Zelinka and Hartmann (2010) showed that perturbed cloud profiles simulated by GCMs were better represented by those following the modified FAT (PHAT) theory than the original FAT theory of Hartmann and Larson (2002). According to the PHAT theory, an increase in the static stability in the upper troposphere under warming results in a smaller rise of clear-sky vertical divergence and convective detrainment levels from those predicted by the FAT theory. Therefore, the cloud anvil temperature becomes slightly warmer than that predicted by the FAT theory. While the quantitative impact of switching from the FAT to PHAT theories is not investigated in the current study, some qualitative discussion may be undertaken. PHAT-cloud PRP is expected to be smaller than FAT-cloud PRP because the cloud altitude feedback would become slightly weaker. As the cloud masking effect is, by definition, not affected by the cloud changes, the PHAT-cloud  $\Delta\text{CRE}$  would decrease by the difference between PHAT-cloud PRP and FAT-cloud PRP and consequently become more negative than the FAT-cloud  $\Delta\text{CRE}$ . The concept of T-FRAT feedback remains valid with the PHAT theory because the cancelling nature of temperature and PHAT-cloud PRP feedbacks remains the same. The slight reduction of cloud amount at the anvil altitudes induced by the PHAT effect, discussed in

section 4a, may slightly change the quantitative aspect of the results.

A potential weak point of the current study is that the cloud modification by the FAT mechanism was made throughout the cloud vertical profiles (except for the lower troposphere), rather than for the cloud anvil alone. While the spatial patterns of the FAT-cloud PRP resemble the spatial patterns of climatological cloud cover at the anvil altitudes, this does not guarantee that the modification of clouds below the anvil level has negligible impact. We tested the sensitivity of TOA radiative flux to the midtropospheric FAT-induced cloud by specifying FAT-induced cloud above 400 hPa and background clouds below that level. In the tropical average, about 83% of FAT-cloud PRP is captured by FAT-induced cloud above 400 hPa (the test was made for 5 years). Therefore, the midtropospheric contribution to the FAT-cloud PRP is minor. Nevertheless, further refinement in constructing FAT-induced cloud should be explored in the future as stated in section 4b. As mentioned briefly in section 3a, Singh and O’Gorman (2012) proposed a theoretically derived vertical coordinate transformation in calculating the upward shift of various atmospheric quantities including temperature and cloud fraction under global warming. Their approach may provide an alternative method to construct FAT-induced cloud with a more solid foundation.

One limitation of our approach is that the PRP diagnosis is impractical for expansion to multimodel analysis. The approach with ISCCP cloud radiative kernels taken by Zelinka et al. (2012a) and Zelinka et al. (2016) is generally better suited for such an application as it requires only model output through a satellite simulator and existing cloud radiative kernels. In addition, the cloud radiative kernels allow the cloud feedback to be computed directly from cloud fraction changes and decomposed into amount, altitude, and optical depth feedbacks. While the positive FAT-cloud feedback in our PRP is consistent with the positive cloud altitude feedback in their analysis, the FAT-induced cloud profile has not been explicitly evaluated by cloud radiative kernels so far. Such an analysis would require additional offline calculation of the ISCCP simulator, or the perturbation must be applied directly to the cloud distribution within the bins of the ISCCP simulator output. While the comparison of different methodologies is certainly of interest, we leave it to future work.

In addition, this article emphasizes the common features in the MIROC5.2-A and HadGEM2-A results. How the new paradigm including the T-FRAT feedback helps us understand the difference between a larger number of models remains to be demonstrated. Nevertheless, by comparing the conventional cloud feedback in the left column and the residual cloud feedback in the right



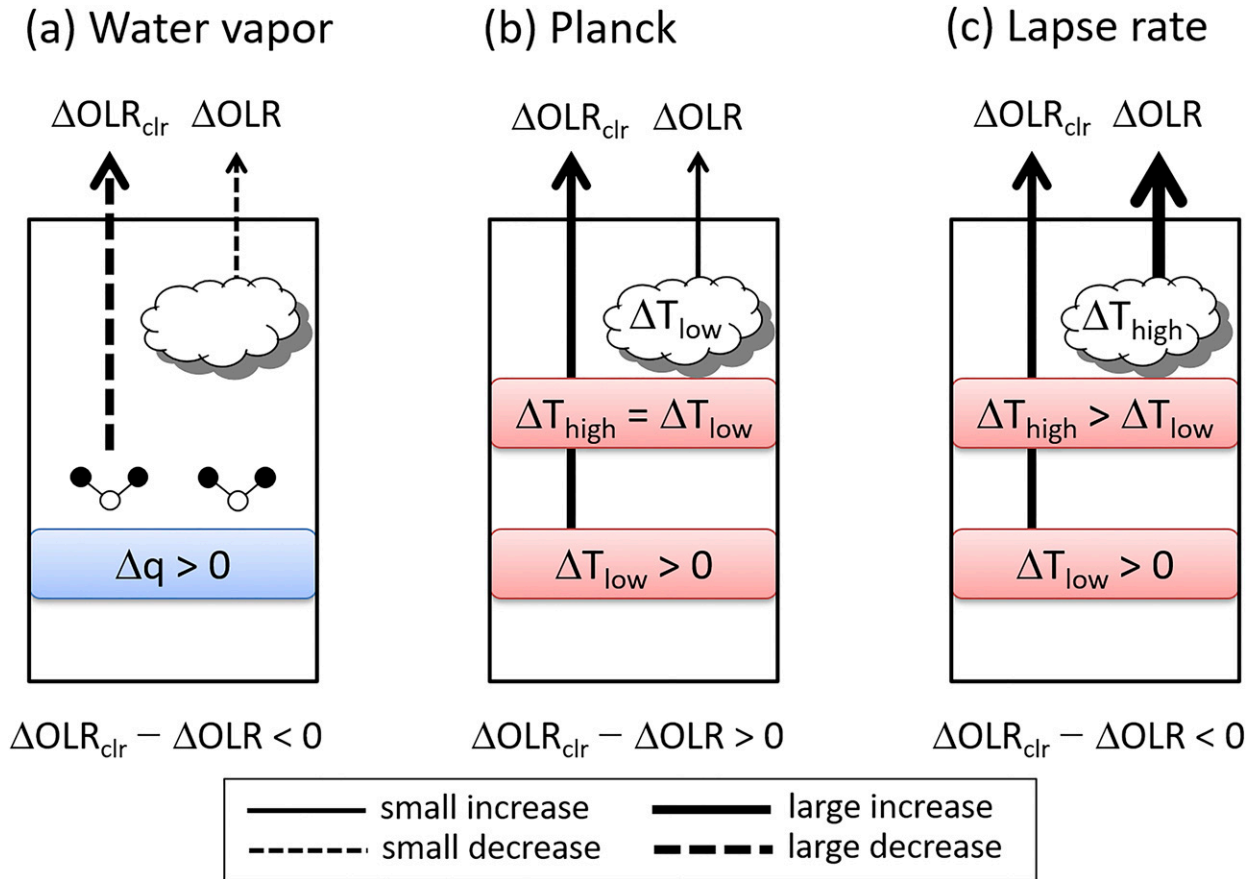


FIG. 10. Schematic illustration of the impact of climatological clouds on noncloud longwave feedbacks (cloud masking) based on the two models analyzed here. Thicker (thinner) arrows indicate stronger (weaker) changes. OLR and  $\text{OLR}_{\text{clr}}$  stand for outgoing longwave radiation and its clear-sky component, respectively; “ $q$ ” and “ $T$ ” denote specific humidity and temperature, respectively; and the subscripts “low” and “high” mean low and high altitudes, respectively. The mathematical expression below each schematic is equal to the cloud masking.

column of Fig. 5b, it becomes clear that much of the difference in conventional LW cloud feedback between MIROC5.2-A and HadGEM2-A arises from the FAT component. About a factor of 3 difference in FAT–cloud PRP between the two models is caused by the difference in climatological clouds and/or the difference in how much the upper troposphere warms and hence how much the climatological clouds shift upward. This result does not mean that the source of the model spread in the cloud feedback for much larger sample sizes also comes from the cloud altitude feedback. Zelinka et al. (2016) concluded that the spread in net (shortwave + LW) cloud feedback over 18 models is dominated by low cloud amount feedback, and the contribution of altitude feedback to the LW nonlow cloud feedback is relatively small compared to amount and optical depth feedbacks.

The current analysis focuses mainly on the radiative impact of tropical cloud response to warming, but a recent study argues that the FAT theory is similarly

applicable to the extratropics (Thompson et al. 2017). The global validity of other aspects of the result should be examined in association with this new global FAT theory in the future.

## 6. Conclusions

The radiative impact of the cloud response following the FAT theory may be described in two different ways. The first description is that the zero-cloud-emission-change feedback resulting from the constant anvil temperature can be considered positive relative to a no-cloud altitude feedback (FAP) case in which the negative temperature feedback would increase upward emission from the cloud. The second description is that the FAT–cloud PRP feedback is positive relative to the FAP–cloud PRP feedback because the FAT-induced cloud altitude is lifted to a pressure at lower emission temperature and thus has an effect of reducing the OLR. These two

(a) MIROC5.2-A: FAT-cloud PRP + cloud masking of T (b) HadGEM2-A: FAT-cloud PRP + cloud masking of T

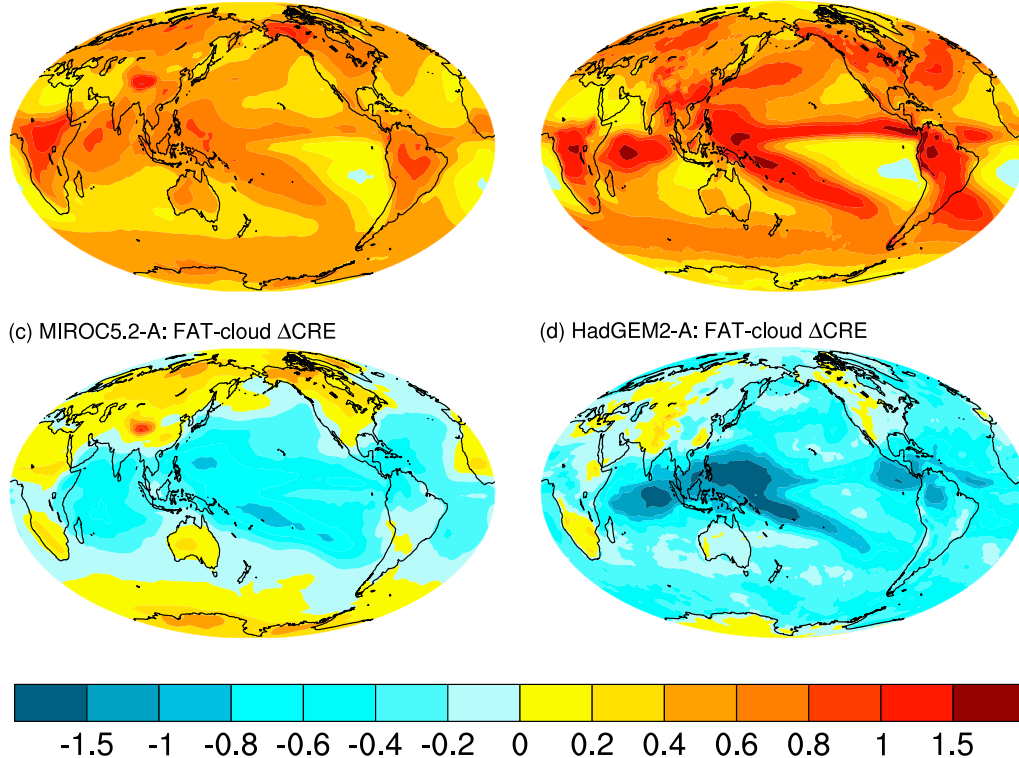


FIG. 11. (a) Sum of FAT-cloud PRP and cloud masking of temperature feedback ( $\text{W m}^{-2} \text{K}^{-1}$ ); (b) as in (a), but for HadGEM2-A; (c) changes in cloud radiative effect ( $\Delta\text{CRE}$ ) for MIROC5.2-A; and (d) as in (c), but for HadGEM2-A.

descriptions are two sides of the same coin: the first description focuses on the thermal radiative damping for the case of both temperature and cloud changes, whereas the second description focuses on the cloud feedback itself. To reconcile these seemingly different descriptions, we first evaluated the radiative impact of the FAT-cloud response in the PRP framework. It was shown that the vertical cloud distribution constructed from the control AMIP clouds following the FAT mechanism reproduces the perturbed AMIP+4K cloud profile well in the tropical average, and it was also shown that the FAT-cloud PRP feedback is positive due to the cloud altitude effect.

The current study proposes a new LW feedback framework in which the cancelling temperature and FAT-cloud PRP feedback terms are combined. The rearrangement of the feedback terms is built upon the Held-Shell framework in which the cancelling lapse rate and water vapor feedback terms were combined. The newly proposed feedback term, the T-FRAT feedback, isolates other feedbacks from those expected from basic physical mechanisms including the FAT theory. The T-FRAT feedback term, which includes feedbacks from constant RH with respect to pressure/altitude and constant clouds with respect to temperature, is less negative than the conventional thermal radiative damping

TABLE 5. A comparison of cloud masking with different cloud climatology and method for MIROC5.2-A ( $\text{W m}^{-2} \text{K}^{-1}$ ).

	Two-sided PRP (AMIP and AMIP+4K clouds)		Radiative kernel (AMIP cloud)		Radiative kernel (AMIP+4K cloud)	
	Global	Tropics	Global	Tropics	Global	Tropics
Water vapor	-0.61	-0.80	-0.58	-0.76	-0.68	-0.91
Planck	0.31	0.35	0.33	0.36	0.34	0.36
Lapse rate	-0.06	-0.12	-0.10	-0.14	-0.04	-0.08
Temperature	0.25	0.23	0.22	0.21	0.30	0.28

(Planck + lapse rate feedback) term. This new framework is more compatible with the description of zero-cloud-emission-change feedback because the residual cloud feedback becomes zero in the case of a purely FAT response.

As the  $\Delta\text{CRE}$ , not the cloud PRP, is the observable quantity, we also evaluated the  $\Delta\text{CRE}$  with the FAT-cloud response. It was shown that the cloud masking effect on the temperature feedback is not a priori positive due to the negative cloud masking of the lapse rate feedback. In addition, understanding the negative cloud masking of temperature feedback requires consideration of the emission-level change by clouds, in addition to the cloud interruption of upwelling LW radiation from below. With that in mind, we argue that “cloud masking” is a misleading term in this context, and instead prefer to describe such effects as the “impact of climatological clouds on noncloud feedbacks” or “cloud climatology effects” for short [similar to the phrase used by Lambert et al. (2015)]. Furthermore, the  $\Delta\text{CRE}$  for the FAT-cloud response was shown to be negative in our models if the impact of climatological clouds on the water vapor feedback is also taken into account.

Is fixed anvil temperature feedback positive, zero, or negative? The FAT-cloud feedback in the PRP framework is positive, consistent with Zelinka and Hartmann (2010). However, we suggest including the fixed anvil temperature feedback as a part of the thermal radiative damping component (together with the conventional temperature feedback), rather than as part of the cloud feedback. This is because the cloud altitude effect under the FAT mechanism makes the thermal radiative damping weaker, and the new framework removes the confounding effects of large opposing terms that cancel each other out and do not contribute to or help to explain the total LW feedback. As a result of this rearrangement of feedback components, the cloud feedback becomes zero under the FAT constraint and negative under the PHAT constraint due to the increase in cloud emission relative to FAT. The remaining cloud feedbacks are ones for which we do not have robust physical explanations, and our T-FRAT method will highlight them and the differences between models and perhaps aid their understanding.

*Acknowledgments.* We are grateful to the editor, Dr. Karen Shell, and Dr. Mark Zelinka and two anonymous reviewers for their many, useful suggestions that helped us to improve the manuscript considerably. The CALIPSO-GOCCP data (Chepfer et al. 2010) were downloaded from <http://climserv.ipsl.polytechnique.fr/cfmip-obs/> on 25 July 2018. We are thankful to the MIROC model development team. We also thank the developers of the freely available software, NCL, SciPy, and SageMath. The MIROC5.2-A simulations were conducted

using the JAMSTEC Earth Simulator 3. At the development stage of this research, MIROC5-A simulations were also conducted using the ITC Fujitsu PRIMEHPC FX10 System at the University of Tokyo. MY thanks Dr. Hiroaki Tatebe for his technical help, Drs. Hideo Shiogama and Tomoo Ogura for providing MIROC5-A ensemble data for comparisons, and Dr. Bjorn Stevens for discussion and useful comment. MY acknowledges support from Integrated Research Program for Advanced Climate Models (TOUGOU program) of MEXT Japan and JSPS KAKENHI Grant JP19K03968. MJW and TA were supported by the Joint U.K. BEIS/Defra Met Office Hadley Centre Climate Programme (GA01101).

## REFERENCES

- Allan, R. P., 2011: Combining satellite data and models to estimate cloud radiative effect at the surface and in the atmosphere. *Meteor. Appl.*, **18**, 324–333, <https://doi.org/10.1002/met.285>.
- Bony, S., and Coauthors, 2006: How well do we understand and evaluate climate change feedback processes? *J. Climate*, **19**, 3445–3482, <https://doi.org/10.1175/JCLI3819.1>.
- , B. Stevens, D. Coppin, T. Becker, K. A. Reed, A. Voigt, and B. Medeiros, 2016: Thermodynamic control of anvil cloud amount. *Proc. Natl. Acad. Sci. USA*, **113**, 8927–8932, <https://doi.org/10.1073/pnas.1601472113>.
- Boucher, O., and Coauthors, 2013: Clouds and aerosols. *Climate Change 2013: The Physical Science Basis*, T. F. Stocker et al., Eds., Cambridge University Press, 571–657.
- Bretherton, C. S., 2015: Insights into low-latitude cloud feedbacks from high-resolution models. *Philos. Trans. Roy. Soc.*, **373A**, 20140415, <https://doi.org/10.1098/rsta.2014.0415>.
- Caldwell, P. M., M. D. Zelinka, K. E. Taylor, and K. Marvel, 2016: Quantifying the sources of intermodel spread in equilibrium climate sensitivity. *J. Climate*, **29**, 513–524, <https://doi.org/10.1175/JCLI-D-15-0352.1>.
- Cess, R. D., 1975: Global climate change: Investigation of atmospheric feedback mechanisms. *Tellus*, **27**, 193–198, <https://doi.org/10.3402/tellusa.v27i3.9901>.
- , and Coauthors, 1990: Intercomparison and interpretation of climate feedback processes in 19 atmospheric general circulation models. *J. Geophys. Res.*, **95**, 16 601–16 615, <https://doi.org/10.1029/JD095iD10p16601>.
- Chae, J. H., and S. C. Sherwood, 2010: Insights into cloud-top height and dynamics from the seasonal cycle of cloud-top heights observed by MISR in the west Pacific region. *J. Atmos. Sci.*, **67**, 248–261, <https://doi.org/10.1175/2009JAS3099.1>.
- Chen, Y. W., T. Seiki, C. Kodama, M. Satoh, A. T. Noda, and Y. Yamada, 2016: High cloud responses to global warming simulated by two different cloud microphysics schemes implemented in the Nonhydrostatic Icosahedral Atmospheric Model (NICAM). *J. Climate*, **29**, 5949–5964, <https://doi.org/10.1175/JCLI-D-15-0668.1>.
- Chepfer, H., S. Bony, D. Winker, G. Cesana, J. L. Dufresne, P. Minnis, C. J. Stubenrauch, and S. Zeng, 2010: The GCM-Oriented CALIPSO Cloud Product (CALIPSO-GOCCP). *J. Geophys. Res.*, **115**, D00H16, <https://doi.org/10.1029/2009JD012251>.
- Colman, R., 2003: A comparison of climate feedbacks in general circulation models. *Climate Dyn.*, **20**, 865–873, <https://doi.org/10.1007/s00382-003-0310-z>.

- , and B. J. McAvaney, 1997: A study of general circulation model climate feedbacks determined from perturbed sea surface temperature experiments. *J. Geophys. Res.*, **102**, 19 383–19 402, <https://doi.org/10.1029/97JD00206>.
- Eitzen, Z. A., K. M. Xu, and T. Wong, 2009: Cloud and radiative characteristics of tropical deep convective systems in extended cloud objects from CERES observations. *J. Climate*, **22**, 5983–6000, <https://doi.org/10.1175/2009JCLI3038.1>.
- Eyring, V., S. Bony, G. A. Meehl, C. A. Senior, B. Stevens, R. J. Stouffer, and K. E. Taylor, 2016: Overview of the Coupled Model Intercomparison Project Phase 6 (CMIP6) experimental design and organization. *Geosci. Model Dev.*, **9**, 1937–1958, <https://doi.org/10.5194/gmd-9-1937-2016>.
- Ferraro, A. J., F. H. Lambert, M. Collins, and G. M. Miles, 2015: Physical mechanisms of tropical climate feedbacks investigated using temperature and moisture trends. *J. Climate*, **28**, 8968–8987, <https://doi.org/10.1175/JCLI-D-15-0253.1>.
- Flato, G., and Coauthors, 2013: Evaluation of climate models. *Climate Change 2013: The Physical Science Basis*, T. F. Stocker et al., Eds., Cambridge University Press, 741–866.
- Hansen, J., A. Lacis, D. Rind, G. Russell, P. Stone, I. Fun, R. Ruedy, and J. Lerner, 1984: Climate sensitivity: Analysis of feedback mechanisms. *Climate Processes and Climate Sensitivity*, *Geophys. Monogr.*, Vol. 29, Amer. Geophys. Union, 130–163, <https://doi.org/10.1029/GM029p0130>.
- Harrop, B. E., and D. L. Hartmann, 2012: Testing the role of radiation in determining tropical cloud-top temperature. *J. Climate*, **25**, 5731–5747, <https://doi.org/10.1175/JCLI-D-11-00445.1>.
- Hartmann, D. L., and K. Larson, 2002: An important constraint on tropical cloud–climate feedback. *Geophys. Res. Lett.*, **29**, 1951, <https://doi.org/10.1029/2002GL015835>.
- Held, I. M., and K. M. Shell, 2012: Using relative humidity as a state variable in climate feedback analysis. *J. Climate*, **25**, 2578–2582, <https://doi.org/10.1175/JCLI-D-11-00721.1>.
- Ingram, W. J., 2010: A very simple model for the water vapour feedback on climate change. *Quart. J. Roy. Meteor. Soc.*, **136**, 30–40, <https://doi.org/10.1002/qj.546>.
- , 2012: Water vapor feedback in a small ensemble of GCMs: Two approaches. *J. Geophys. Res.*, **117**, D12114, <https://doi.org/10.1029/2011JD017221>.
- , 2013: Some implications of a new approach to the water vapour feedback. *Climate Dyn.*, **40**, 925–933, <https://doi.org/10.1007/s00382-012-1456-3>.
- Jones, C. D., and Coauthors, 2011: The HadGEM2-ES implementation of CMIP5 centennial simulations. *Geosci. Model Dev.*, **4**, 543–570, <https://doi.org/10.5194/gmd-4-543-2011>.
- Koll, D. D. B., and T. W. Cronin, 2018: Earth's outgoing longwave radiation linear due to H<sub>2</sub>O greenhouse effect. *Proc. Natl. Acad. Sci. USA*, **115**, 10 293–10 298, <https://doi.org/10.1073/pnas.1809868115>.
- Kuang, Z. M., and D. L. Hartmann, 2007: Testing the fixed anvil temperature hypothesis in a cloud-resolving model. *J. Climate*, **20**, 2051–2057, <https://doi.org/10.1175/JCLI4124.1>.
- Lambert, F. H., and P. C. Taylor, 2014: Regional variation of the tropical water vapor and lapse rate feedbacks. *Geophys. Res. Lett.*, **41**, 7634–7641, <https://doi.org/10.1002/2014GL061987>.
- , M. J. Webb, M. Yoshimori, and T. Yokohata, 2015: The cloud radiative effect on the atmospheric energy budget and global mean precipitation. *Climate Dyn.*, **44**, 2301–2325, <https://doi.org/10.1007/s00382-014-2174-9>.
- Li, Y., P. Yang, G. R. North, and A. Dessler, 2012: Test of the fixed anvil temperature hypothesis. *J. Atmos. Sci.*, **69**, 2317–2328, <https://doi.org/10.1175/JAS-D-11-0158.1>.
- Martin, G. M., and Coauthors, 2011: The HadGEM2 family of Met Office Unified Model climate configurations. *Geosci. Model Dev.*, **4**, 723–757, <https://doi.org/10.5194/gmd-4-723-2011>.
- Nitta, T., and Coauthors, 2014: Representing variability in subgrid snow cover and snow depth in a global land model: Offline validation. *J. Climate*, **27**, 3318–3330, <https://doi.org/10.1175/JCLI-D-13-00310.1>.
- , K. Yoshimura, and A. Abe-Ouchi, 2017: Impact of Arctic wetlands on the climate system: Model sensitivity simulations with the MIROC5 AGCM and a snow-fed wetland scheme. *J. Hydrometeorol.*, **18**, 2923–2936, <https://doi.org/10.1175/JHM-D-16-0105.1>.
- Ogura, T., and Coauthors, 2017: Effectiveness and limitations of parameter tuning in reducing biases of top-of-atmosphere radiation and clouds in MIROC version 5. *Geosci. Model Dev.*, **10**, 4647–4664, <https://doi.org/10.5194/gmd-10-4647-2017>.
- Ohno, T., and M. Satoh, 2018: Roles of cloud microphysics on cloud responses to sea surface temperatures in radiative-convective equilibrium experiments using a high-resolution global non-hydrostatic model. *J. Adv. Model. Earth Syst.*, **10**, 1970–1989, <https://doi.org/10.1029/2018MS001386>.
- Po-Chedley, S., K. C. Armour, C. M. Bitz, M. D. Zelinka, B. D. Santer, and Q. Fu, 2018: Sources of intermodel spread in the lapse rate and water vapor feedbacks. *J. Climate*, **31**, 3187–3206, <https://doi.org/10.1175/JCLI-D-17-0674.1>.
- Randall, D. A., and Coauthors, 2007: Climate models and their evaluation. *Climate Change 2007: The Physical Science Basis*, S. Solomon et al., Eds., Cambridge University Press, 589–662.
- Seeley, J. T., N. Jeevanjee, and D. M. Romps, 2019a: FAT or FiTT: Are anvil clouds or the tropopause temperature invariant? *Geophys. Res. Lett.*, **46**, 1842–1850, <https://doi.org/10.1029/2018GL080096>.
- , —, W. Langhans, and D. M. Romps, 2019b: Formation of tropical anvil clouds by slow evaporation. *Geophys. Res. Lett.*, **46**, 492–501, <https://doi.org/10.1029/2018GL080747>.
- Shell, K. M., J. T. Kiehl, and C. A. Shields, 2008: Using the radiative kernel technique to calculate climate feedbacks in NCAR's Community Atmospheric Model. *J. Climate*, **21**, 2269–2282, <https://doi.org/10.1175/2007JCLI2044.1>.
- Sherwood, S. C., W. Ingram, Y. Tsushima, M. Satoh, M. Roberts, P. L. Vidale, and P. A. O'Gorman, 2010: Relative humidity changes in a warmer climate. *J. Geophys. Res.*, **115**, D09104, <https://doi.org/10.1029/2009JD012585>.
- Singh, M. S., and P. A. O'Gorman, 2012: Upward shift of the atmospheric general circulation under global warming: Theory and simulations. *J. Climate*, **25**, 8259–8276, <https://doi.org/10.1175/JCLI-D-11-00699.1>.
- Soden, B. J., and I. M. Held, 2006: An assessment of climate feedbacks in coupled ocean–atmosphere models. *J. Climate*, **19**, 3354–3360, <https://doi.org/10.1175/JCLI3799.1>.
- , and G. A. Vecchi, 2011: The vertical distribution of cloud feedback in coupled ocean–atmosphere models. *Geophys. Res. Lett.*, **38**, L12704, <https://doi.org/10.1029/2011GL047632>.
- , A. J. Broccoli, and R. S. Hemler, 2004: On the use of cloud forcing to estimate cloud feedback. *J. Climate*, **17**, 3661–3665, [https://doi.org/10.1175/1520-0442\(2004\)017<3661:OTUOCF>2.CO;2](https://doi.org/10.1175/1520-0442(2004)017<3661:OTUOCF>2.CO;2).
- , I. M. Held, R. Colman, K. M. Shell, J. T. Kiehl, and C. A. Shields, 2008: Quantifying climate feedbacks using radiative kernels. *J. Climate*, **21**, 3504–3520, <https://doi.org/10.1175/2007JCLI2110.1>.
- Tatebe, H., Y. Tanaka, Y. Komuro, and H. Hasumi, 2018: Impact of deep ocean mixing on the climatic mean state in the

- Southern Ocean. *Sci. Rep.*, **8**, 14479, <https://doi.org/10.1038/s41598-018-32768-6>.
- Taylor, K. E., M. Crucifix, P. Braconnot, C. D. Hewitt, C. Doutriaux, A. J. Broccoli, J. F. Mitchell, and M. J. Webb, 2007: Estimating shortwave radiative forcing and response in climate models. *J. Climate*, **20**, 2530–2543, <https://doi.org/10.1175/JCLI4143.1>.
- , R. J. Stouffer, and G. A. Meehl, 2012: An overview of CMIP5 and the experiment design. *Bull. Amer. Meteor. Soc.*, **93**, 485–498, <https://doi.org/10.1175/BAMS-D-11-00094.1>.
- Thompson, D. W. J., S. Bony, and Y. Li, 2017: Thermodynamic constraint on the depth of the global tropospheric circulation. *Proc. Natl. Acad. Sci. USA*, **114**, 8181–8186, <https://doi.org/10.1073/pnas.1620493114>.
- Watanabe, M., and Coauthors, 2010: Improved climate simulation by MIROC5: Mean states, variability, and climate sensitivity. *J. Climate*, **23**, 6312–6335, <https://doi.org/10.1175/2010JCLI3679.1>.
- Wetherald, R. T., and S. Manabe, 1988: Cloud feedback processes in a general circulation model. *J. Atmos. Sci.*, **45**, 1397–1416, [https://doi.org/10.1175/1520-0469\(1988\)045<1397:CFPIAG>2.0.CO;2](https://doi.org/10.1175/1520-0469(1988)045<1397:CFPIAG>2.0.CO;2).
- Xu, K. M., T. M. Wong, B. A. Wielicki, L. Parker, and Z. A. Eitzen, 2005: Statistical analyses of satellite cloud object data from CERES. Part I: Methodology and preliminary results of the 1998 El Niño/2000 La Niña. *J. Climate*, **18**, 2497–2514, <https://doi.org/10.1175/JCLI3418.1>.
- , T. Wong, B. A. Wielicki, L. Parker, B. Lin, Z. A. Eitzen, and M. Branson, 2007: Statistical analyses of satellite cloud object data from CERES. Part II: Tropical convective cloud objects during 1998 El Niño and evidence for supporting the fixed anvil temperature hypothesis. *J. Climate*, **20**, 819–842, <https://doi.org/10.1175/JCLI4069.1>.
- Yoshimori, M., T. Yokohata, and A. Abe-Ouchi, 2009: A comparison of climate feedback strength between CO<sub>2</sub> doubling and LGM experiments. *J. Climate*, **22**, 3374–3395, <https://doi.org/10.1175/2009JCLI2801.1>.
- , J. C. Hargreaves, J. D. Annan, T. Yokohata, and A. Abe-Ouchi, 2011: Dependency of feedbacks on forcing and climate state in physics parameter ensembles. *J. Climate*, **24**, 6440–6455, <https://doi.org/10.1175/2011JCLI3954.1>.
- Zelinka, M. D., and D. L. Hartmann, 2010: Why is longwave cloud feedback positive? *J. Geophys. Res.*, **115**, D16117, <https://doi.org/10.1029/2010JD013817>.
- , and —, 2011: The observed sensitivity of high clouds to mean surface temperature anomalies in the tropics. *J. Geophys. Res.*, **116**, D23103, <https://doi.org/10.1029/2011JD016459>.
- , S. A. Klein, and D. L. Hartmann, 2012a: Computing and partitioning cloud feedbacks using cloud property histograms. Part I: Cloud radiative kernels. *J. Climate*, **25**, 3715–3735, <https://doi.org/10.1175/JCLI-D-11-00248.1>.
- , —, and —, 2012b: Computing and partitioning cloud feedbacks using cloud property histograms. Part II: Attribution to changes in cloud amount, altitude, and optical depth. *J. Climate*, **25**, 3736–3754, <https://doi.org/10.1175/JCLI-D-11-00249.1>.
- , C. Zhou, and S. A. Klein, 2016: Insights from a refined decomposition of cloud feedbacks. *Geophys. Res. Lett.*, **43**, 9259–9269, <https://doi.org/10.1002/2016GL069917>.
- Zhang, M. H., J. J. Hack, J. T. Kiehl, and R. D. Cess, 1994: Diagnostic study of climate feedback processes in atmospheric general circulation models. *J. Geophys. Res.*, **99**, 5525–5537, <https://doi.org/10.1029/93JD03523>.